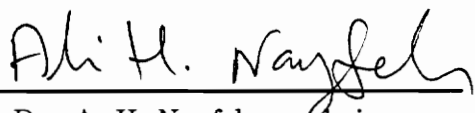# Nonlinear Dynamics of Systems Involving Widely Spaced Frequencies

by
Samir Ali Nayfeh

Thesis submitted to the faculty of the
Virginia Polytechnic Institute and State University
in partial fulfillment of the requirements for the degree of
Master of Science
in
Engineering Mechanics

Approved:

_____
Dr. A. H. Nayfeh, co-chairman

_____
Dr. D. T. Mook, co-chairman

_____
Dr. S. L. Hendricks

_____
Dr. M. W. Hyer

_____
Dr. L. G. Kraige

April 1993
Blacksburg, Virginia
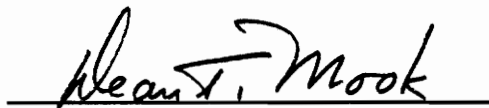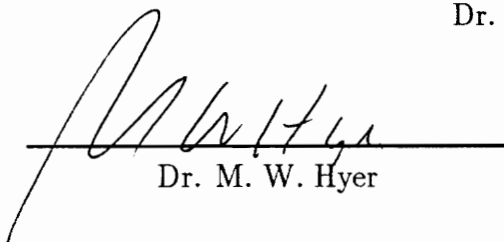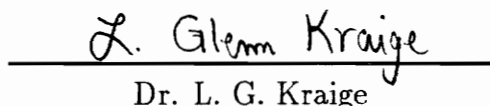
Nonlinear Dynamics of Systems Involving Widely Spaced Frequencies

by

Samir Ali Nayfeh

Drs. A. H. Nayfeh and D. T. Mook, Co-chairmen

Engineering Science and Mechanics

ABSTRACT

This document focuses on the dynamics of nonlinear oscillatory systems involving widely spaced frequencies. First, experiments on the forced oscillations of a cantilever beam with a circular cross-section are presented. The beam is excited near its fifth natural frequency but sustained large-amplitude oscillations of the first mode accompanied by modulated oscillations of the fifth mode occur. Thus, energy is transferred from the fifth to the first mode of the beam, whose natural frequencies are roughly in the ratio of 60:1.

Some simple two-degree-of-freedom systems are studied in an effort to explain the strong nonlinear coupling between modes with widely spaced frequencies. In these systems, the coupling is found to give rise to some novel phenomena including static displacements or sustained oscillations of the low-frequency mode in response to a high-frequency excitation.

The possibility that resonances may occur between a high-frequency excitation and a single low-frequency mode is then investigated. A single-degree-of-freedom oscillator driven at a frequency much higher than its natural frequency is analyzed. It is found that, if the excitation is modulated, resonant excitation of the oscillator may occur.

ACKNOWLEDGEMENTS

I would like to thank committee co-chairmen, Drs. A. H. Nayfeh and D. T. Mook, who taught me at least *1,001 Fun Facts About Nonlinear Dynamics*. The remaining committee members, Drs. Hendricks, Hyer, and Kraige, are to be commended for reading the thesis and providing valuable comments. Moreover, I thank each member of the committee for providing me with excellent course instruction during my undergraduate and graduate years at VPI & SU.

I owe some thanks to my colleagues, Ossama Ashour, Balakumar Balachandran, Wayne Krieder, and Mahmoud Tabador, some of whom stayed awake through the defense. I owe more thanks to Tony Anderson and Kyoyul Oh for engaging me in incessant technical discussions which were most helpful in the development of this thesis.

Most of all, I would like to thank my parents, Ali and Inam Nayfeh, for providing me with guidance, unconditional support, endless affection, clean clothes, and hot food for twenty-some odd years.

CONTENTS

CHAPTER 1

Introduction

In this thesis, we study nonlinear systems in which the ratio of any two frequencies is very small. By 'frequencies', we mean any frequency involved in the system whether it be the natural frequency of a mode or an excitation frequency. In such systems, a range of phenomena may occur which cannot occur in systems where all frequencies are of the same order. Of primary interest is the transfer of energy between oscillations occurring at widely spaced frequencies.

1.1   Motivation

Modern flexible structures typically have several modes with very low natural frequencies. Because these structures are flexible, large-amplitude vibrations may occur, and geometric and other nonlinearities become significant. The nonlinearity couples the modes and can lead to modal interactions where energy is transferred between modes. Previous research on modal interactions has shown that they may occur when a special relationship between the natural frequencies of two or more modes and the excitation frequency exists. Some recent experiments indicate, however, that a previously undocumented type of modal interaction can occur between modes whose frequencies are in the ratio of roughly 1:20 and smaller. A theoretical and experimental study of

this interaction between widely spaced modes is presented in Chapters 2 through 4 of this thesis.

In many engineering applications, vibrations caused by rotating machinery are unavoidable. Often, supporting structures are isolated from this vibration by mounting the machinery on soft springs in order to form a supporting system with a natural frequency much lower than the frequency of operation of the machinery. Such an isolator may be modeled as a one-degree-of-freedom system with an excitation applied at a frequency much higher than its own natural frequency. If the system is linear, it operates far from resonance and the force transmitted to the structure is small. If, however, nonlinearities are present in the support and the machine operates in a nonstationary manner, dangerous resonances may occur. We discuss this possibility in Chapter 5 of this thesis.

1.2   Systems With Frequencies of the Same Order

In this section, we briefly discuss the dynamics of lightly damped weakly nonlinear systems where all frequencies are of the same order. We note that any system with smooth nonlinearities may be cast as a weakly nonlinear system for small enough displacements. Also, if all of the frequencies are of the same order, we can nondimensionalize them so that they are all $O(1)$.

We consider a system of second-order oscillators of the form

$$\ddot{u}_i + \omega_i^2 u_i = \epsilon f_i(u, \dot{u}, t) \tag{1.1}$$

where the f_i represent the nonlinearity, damping, excitations, and other perturbations. That these perturbations are small is made explicit by using a small dimensionless quantity ϵ as coefficient of the f_i. Some insight into the dynamics of the system can be gained by introducing the variation-of-parameters transformation

$$u_i = a_i(t)\cos(\phi_i(t)) \tag{1.2}$$

$$\dot{u}_i = -\omega_i a_i(t)\sin(\phi_i(t)) \tag{1.3}$$

where $\phi_i(t) = \omega_i t + \beta_i(t)$ to obtain

$$\dot{a}_i = -\frac{\epsilon}{\omega_i} f_i(a_j \cos \phi_j, -\omega_j \dot{a}_j \sin \phi_j, t) \sin \phi_i \qquad (1.4)$$

$$a_i \dot{\beta}_i = -\frac{\epsilon}{\omega_i} f_i(a_j \cos \phi_j, -\omega_j \dot{a}_j \sin \phi_j, t) \cos \phi_i \qquad (1.5)$$

Under the assumption that the ω_i are not small, we see from Eqs. (1.4) and (1.5) that the $\dot{a}_i$ and $\dot{\beta}_i$ are small and therefore conclude that the a_i and β_i are slowly varying. That is, the a_i and β_i evolve much more slowly than the u_i. This fact is very useful in the study of weakly nonlinear systems and most perturbation methods are built upon it. In the method of averaging, we classify terms as being either slowly or rapidly varying and in the method of multiple time scales, we refer to terms as evolving on either the slow or fast scales.

Terms on the right-hand sides of Eqs. (1.4) and (1.5) must act over a long period of time in order to have a large effect on the a_i and β_i. Because rapidly varying terms change sign at a high frequency, they have little net effect. In the averaging approximation, these rapidly varying terms are smoothed away, yielding a simpler mathematical representation of the system.

The only terms that have a large effect and remain after the averaging approximation are the slowly varying terms on the right-hand sides of Eqs. (1.4) and (1.5). Thus, in Eqs. (1.4) and (1.5) only the terms in f_i of nearly the same frequency and phase as $\sin \phi_i$ and $\cos \phi_i$, respectively, have large effects. These terms are commonly referred to as secular or small-divisor terms.

This discussion forms a framework for the understanding of nonlinear resonance phenomena. Large responses to small excitations can occur when one or more excitation frequency, the values of the ω_i, and the form of f_j are such that terms of frequency nearly equal to ω_j appear. Strong coupling between modes (modal interactions) can occur when the values of the ω_i and the form of f_j are such that terms with frequency nearly equal to ω_j appear.

1.3 Modal Interactions

Nonlinear modal interactions have been the subject of a great deal of recent research. It has been found that, in weakly-nonlinear systems where there exists a special relationship between two or more natural frequencies of the linear modes and an excitation frequency, the long-time response can contain large contributions from several modes. In an analytical model, it is necessary to include all of the modes that participate significantly in the response and the larger the number of modes is, the more complicated the dynamics of the system can be. More importantly, modal interactions can lead to dangerously large responses in modes that are predicted by linear analyses to have insignificant response amplitudes.

Most of the research on modal interactions focuses on internal or autoparametric resonances in systems where the linear natural frequencies ω_i are commensurate or nearly commensurate. The types of possible autoparametric resonances depend on the degree of the nonlinearity and the number of modes involved. When the nonlinearity is cubic, to the first approximation, autoparametric resonances may occur if $\omega_n \approx \omega_m$, $\omega_n \approx 3\omega_m$, $\omega_n \approx |\pm 2\omega_m \pm \omega_k|$, or $\omega_n \approx |\pm \omega_m \pm \omega_k \pm \omega_l|$. If quadratic nonlinearities are added, additional resonances may occur if $\omega_n \approx 2\omega_m$ or $\omega_n \approx \omega_m + \omega_k$. These autoparametric resonances have been successfully treated with perturbation methods (Nayfeh, 1973, 1981; Crespo da Silva, 1980; Bajaj and Johnson, 1990). There also exists a large body of experimental results which are in good general agreement with the perturbation results (Nayfeh and Mook, 1979; Nayfeh and Balachandran, 1989). Autoparametric resonances may provide a coupling or an energy exchange between the modes of a system. Consequently, excitation of a high-frequency mode may produce a large-amplitude response in a low-frequency mode involved with it in an autoparametric resonance.

In externally excited multi-degree-of-freedom systems, combination resonances may occur in response to a simple-harmonic external excitation of frequency Ω. The type of combination resonance that can be excited depends on the degree of the

nonlinearity, the number of modes involved, and Ω. For a cubic nonlinearity, to the first approximation, combination resonances may occur if $\Omega \approx \frac{1}{2}|\pm\omega_m \pm \omega_k|$, $\Omega \approx |\pm 2\omega_m \pm \omega_k|$, or $\Omega \approx |\pm\omega_m \pm \omega_k \pm \omega_l|$. If quadratic nonlinearities are added, additional combination resonances may occur if $\Omega \approx |\pm\omega_m \pm \omega_k|$. Thus, a high-frequency excitation may produce large-amplitude responses in low-frequency modes that are involved in the combination resonance. Dugundji and Mukhopadhyay (1973) conducted experiments on a cantilever beam subjected to an external base excitation at a frequency close to the sum of the natural frequencies of the first bending and first torsional modes, which were approximately in the ratio of one to 18. They found that the high-frequency excitation can produce a large-amplitude response in the low-frequency (first bending) mode.

In parametrically excited systems, modal interactions can occur when the excitation frequency is near the sum or difference of two or more linear natural frequencies. These so-called combination resonances have been studied extensively in the literature (e.g., Nayfeh and Mook, 1979; Schmidt and Tondl, 1986; Nayfeh and Jebril, 1987). Again, combination resonances can lead to interactions between high- and low-frequency modes.

Often, when the response of a system becomes chaotic, low-frequency modes can be excited. Haddow and Hasan (1988) conducted an experiment by parametrically exciting a cantilever beam near twice the natural frequency of its fourth mode. They found that, as the excitation frequency was decreased, a planar periodic response consisting essentially of the fourth mode lost stability, giving way to a nonplanar chaotic motion. They observed that, as a result, the energy seemed to cascade down through the modes, resulting eventually in a very low-frequency component in the steady-state response. Burton and Kolowith (1988) conducted an experiment similar to that of Haddow and Hasan. In certain regions of the parameter space, they observed chaotic motions where the lowest seven in-plane bending modes as well as the first torsional mode were present in the response. Cusumano and Moon (1989) conducted an ex-

periment with an externally excited cantilever beam. They observed a cascading of energy to low-frequency components in the transition to chaotic non-planar motions.

A recent study suggests that another type of interaction may occur between high- and low-frequency modes. Anderson, Balachandran, and Nayfeh (1992) conducted experiments on a parametrically excited cantilever. They found that interactions occur between two high-frequency modes and the first mode. The presence of the first mode is accompanied by slow modulations of the amplitudes and phases of the high-frequency modes. The frequency of the modulations is equal to the frequency of oscillation of the first mode. This indicates that the mechanism for the excitation of the first mode is neither a classical internal resonance nor an external or parametric combination resonance involving the first mode. Rather, it seems that slow modulation of the high-frequency modes allows energy to be transferred to the first mode.

Anderson, Nayfeh, and Balachandran (1993) employed an averaging scheme to analyze the energy transfer phenomenon observed in their experiment. In their analysis, the two high-frequency modal coordinates were considered to be rapidly varying quantities while the low-frequency modal coordinate was treated as slowly varying. They found that modulation of the high-frequency modes is necessary for excitation of the low-frequency mode to occur.

1.4   Overview

This thesis focuses on means by which high-frequency sources can lead to low-frequency oscillations. We present some experimental results and then discuss ways in which the method of multiple scales and the method of averaging can be used to study systems with widely spaced frequencies.

An experimental study of the response of an axially symmetric cantilever beam to planar external excitations is presented in Chapter 2. When the beam is excited near one of its high natural frequencies, large first-mode responses accompanied by slow

modulations of the amplitudes and phases of the high-frequency modes are observed. This is an example of the energy transfer from high- to low-frequency modes reported in Anderson, Balachandran, and Nayfeh (1992).

To investigate this phenomenon, we study some simple two-degree-of-freedom nonlinear systems with widely spaced frequencies. In Chapter 3, we use the method of multiple scales to study a system with quadratic nonlinearities. We find that this system does indeed exhibit the energy-transfer phenomenon. Next, we investigate the possibility of energy transfer from low- to high-frequency modes and find that it will not generally occur.

In Chapter 4, we use the method of averaging to study a system with cubic nonlinearities. We find that this system may also exhibit the energy-transfer phenomenon from high- to low-frequency modes. The dynamics of this system are somewhat more complicated than the dynamics of the system with quadratic nonlinearities studied in Chapter 3. Various nonlinear phenomena, such as period-doubling bifurcations culminating in chaos, symmetry-breaking bifurcations, the existence of multiple attractors, and the merging of attractors are found to occur.

In Chapter 5, we study a one-degree-of freedom system subjected to a modulated excitation whose basic frequency is much higher than the natural frequency of the system. We find that when a nonlinear system is subjected to an excitation with a frequency much higher than its own natural frequency, the system averages the excitation, smoothing away the high-frequency carrier but leaving behind any low-frequency variations. Under some conditions, these low-frequency components may resonantly excite the system.

CHAPTER 2

Experiments on a Cantilever Beam

2.1 Introduction

In this chapter, we present experimental results for an externally excited, circular cross-section, cantilever beam. Because of the axial symmetry, one-to-one autoparametric resonances occur at each natural frequency of the beam. The mode in the plane of the excitation can interact with the out-of-plane mode at the same natural frequency and the result is a non-planar whirling motion. This modal interaction has been the subject of numerous studies (Haight and King, 1972; Hyer, 1979; Crespo da Silva, 1980; Pai and Nayfeh, 1990; Shyu, Mook, and Plaut, 1993).

In this study, we focus on the dynamics that occur when we excite the beam at high frequencies. It is found that when the beam is excited near the natural frequency of its third or any higher mode, a large first-mode response occurs. Moreover, the degree of the coupling between the first mode and the higher modes is observed to increase as progressively higher modes of the beam are excited. As in the study of Anderson and coworkers, the appearance of the first mode is accompanied by modulations of the amplitudes and phases of the high-frequency modes. The results presented here for the case where the excitation frequency is near the fifth natural frequency of the beam are representative of the behavior of the beam for excitation frequencies near

Table 2.1   The first five natural frequencies of the test specimen

Mode	Natural Frequency (Hz)
1	1.303 ± 0.005
2	9.049 ± 0.005
3	25.564 ± 0.005
4	50.213 ± 0.007
5	83.150 ± 0.011

any of its higher natural frequencies.

2.2   Experimental Setup

We present the results of experiments conducted on a slender, circular cross-section, steel, cantilever beam. The length of the cantilever is 34.5" and the diameter of its cross-section is 0.0625". The first five linear natural frequencies of the beam, as determined by examination of the frequency spectra of decaying free oscillations, are shown in Table 2.1.

Figure 2.1 is a schematic diagram of the experimental setup. A vertical beam is clamped to a 100-lb shaker that supplies a simple-harmonic motion at the base so that an external (i.e., transverse to the axis of the beam) excitation is applied. The excitation is monitored by means of an accelerometer mounted to the shaker head. The motion of the tip of the beam is measured by two linear-array cameras, one oriented to measure the motion in the plane of the excitation (camera 0) and the other oriented to measure the motion out of the plane of the excitation (camera 1).

The linear-array camera system, developed by Colbert (1990), employs a hardware-implemented peak detector to determine the location of the target in real-time. At a specified sampling frequency, it returns two eleven-bit numbers representing the displacements of the tip of the beam in the in-plane and out-of-plane directions. This
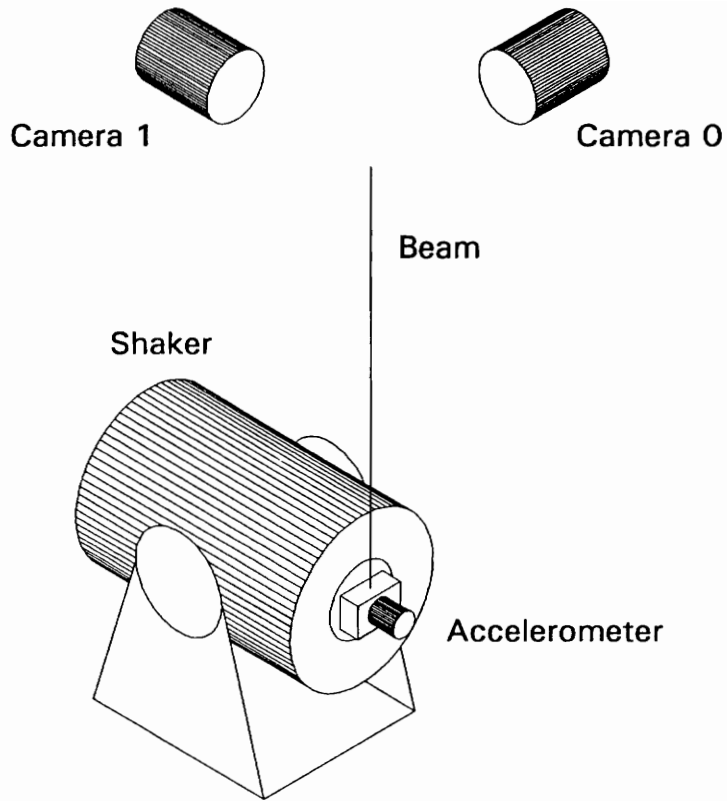
Fig. 2.1   Experimental setup

data is passed real-time to a personal computer where it is displayed, processed, and stored.

Because the beam constitutes a weakly nonlinear system, its response $w(x, t)$ is assumed to be composed of a combination of its linear mode shapes $\phi_n(x)$ in the form

$$w(x, t) = \sum_n u_n(t)\phi_n(x)$$

In addition, if a response spectrum of the beam contains a single peak near its fifth natural frequency, we interpret the peak to represent a periodic response that is composed mostly of the fifth mode. If the response is periodic, the modal amplitudes can be determined directly from an FFT computed with flat-top windowing. If the amplitude and phase of a mode are modulated, the frequency response will contain side bands and the modal amplitude cannot simply be read from an FFT. In this case, we run the signal through a band-pass filter to eliminate the contributions of any other modes and then directly compute the root-mean-square amplitude of the remaining signal.

It should be noted that the methods for decomposition of the response into various modes outlined in the preceding paragraph can fail for a variety of reasons. The basic assumption that the response of the system is composed of a combination of linear mode shapes may be invalid. More commonly, the response of the beam may have a broad-band character and the modal responses cannot be separated in the frequency domain. Even in the case of periodic responses, if the response is sufficiently distorted from a simple sinusoid, its frequency spectrum will contain large peaks at harmonics of its fundamental frequency that must be considered in order to obtain an accurate measure of the mode's response. For most weakly nonlinear systems (including the one considered here), however, these problems don't often arise and their response can be easily decomposed into linear mode shapes.

2.3 Frequency-Response Curves

We present frequency-response curves for the fifth in-plane and out-of-plane modes of the cantilever beam. The excitation level was held constant at $2.00g$ rms (where g is the acceleration of gravity) and the excitation frequency was varied in the neighborhood of the fifth natural frequency. Changes in the excitation frequency were made very gradually and, at each excitation frequency, transients were allowed to die out before the amplitude of the response was recorded. The data in the plots is a composite of the responses obtained by performing both forward and backward frequency sweeps. In addition, to ensure that even isolated branches of the frequency-response curves were located, we performed a third sweep where, at increments in the excitation frequency, we applied several disturbances to the beam in an effort to find all possible long-time responses.

The results of this procedure are shown in Fig. 2.2. Well away from the fifth natural frequency, the only possible response is planar and periodic. The response of the beam is strictly in the plane of the excitation and a visual inspection of the motion indicates that the response is composed almost entirely of the fifth mode. This is confirmed by examination of the response spectrum which shows only a single peak at the excitation frequency.

As the frequency of excitation is swept upward from well below the fifth natural frequency, a jump occurs from a planar-periodic to a non-planar strongly modulated motion. Here, visual inspection of the response clearly detects the modulation of the response of the fifth mode as well as the presence of a low-frequency component in the response.

Increasing the excitation frequency further, we observe a jump to a non-planar weakly modulated whirling motion. Again, visual inspection of the motion clearly reveals a large low-frequency component in the response. In this case, however, visual inspection does not detect any modulation of the fifth mode. A more detailed discussion of both the weakly and strongly modulated motions follows.
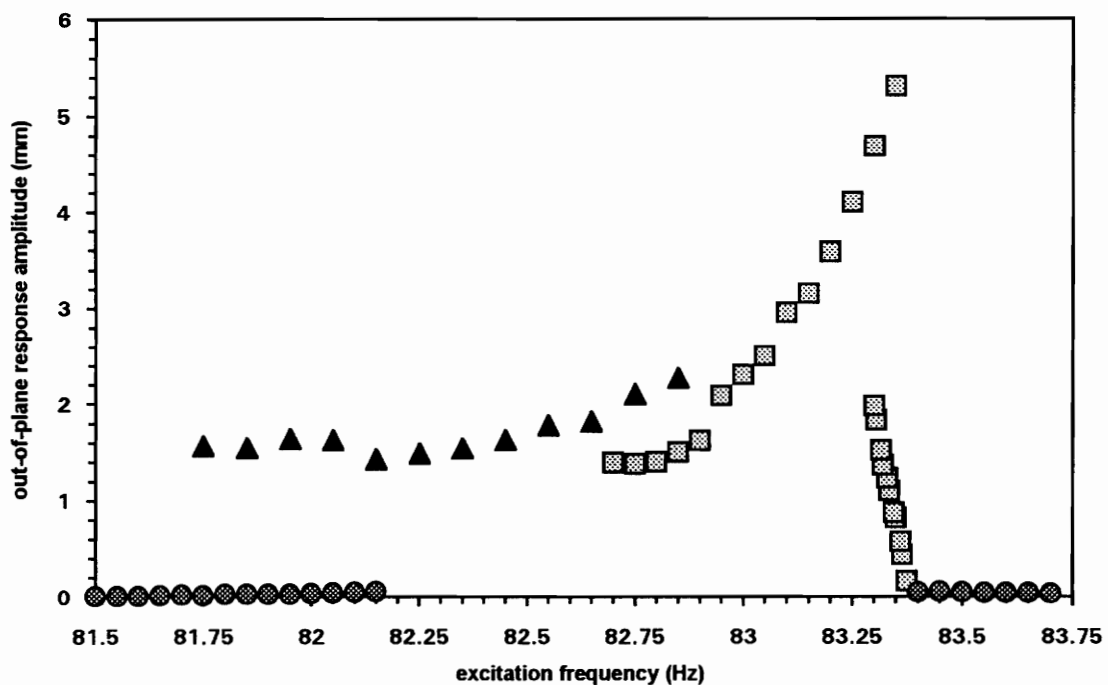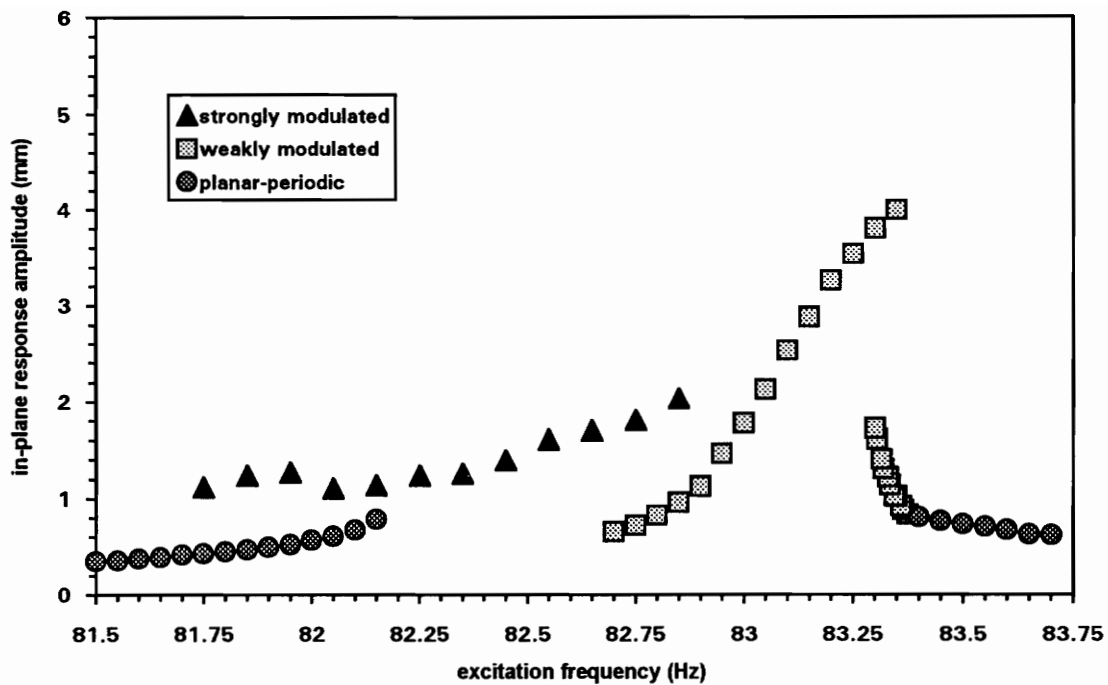
Fig. 2.2   Frequency-response curves of the fifth mode for an excitation amplitude of $2.00g$ rms

2.4 Weakly Modulated Motion

As mentioned in the preceding section, the observed weakly modulated responses contain a large low-frequency component superimposed on a nearly constant amplitude fifth-mode whirling motion. Typical time traces of in-plane and out-of-plane responses of this type are shown in Fig. 2.3(a). Visual inspection of these plots does not readily reveal any modulation of either the high- or low-frequency components of the response.

A typical FFT of this type of response is shown in Fig. 2.4. The FFT shows two main peaks, one at the frequency of the excitation (near the fifth natural frequency) and the other at the natural frequency of the first mode. The asymmetric side-band structure around the peak corresponding to the fifth mode indicates that the response of the fifth mode is amplitude- and phase-modulated. Moreover, the frequency spacing between the fifth-mode peak and its side bands is equal to the first natural frequency, confirming that the frequency of modulation of the fifth-mode response is equal to the natural frequency of the first mode.

As indicated by the dense set of side bands clustered around the peak at the first natural frequency, the response of the first mode is also modulated. Examination of the time-domain data from which this FFT was computed, shown in Fig. 2.3(b), confirms that the amplitude of the first-mode response is not constant. The time traces in Fig. 2.3(b) contain 170 seconds of data, illustrating the extremely slow variation of the amplitude of the first mode.

It should be noted that the samples shown are not long enough to give a good indication of how the first-mode response amplitude varies. Unfortunately, we are currently unable to store longer samples of data. Long-time visual observation reveals no simple trend or periodicity in the response. Because of the extremely slow and erratic evolution of the first-mode response, it is difficult to obtain an estimate of its amplitude in an average sense. The time traces shown in Fig. 2.3(a) do however give an indication that the response of the first mode can in many cases be several times
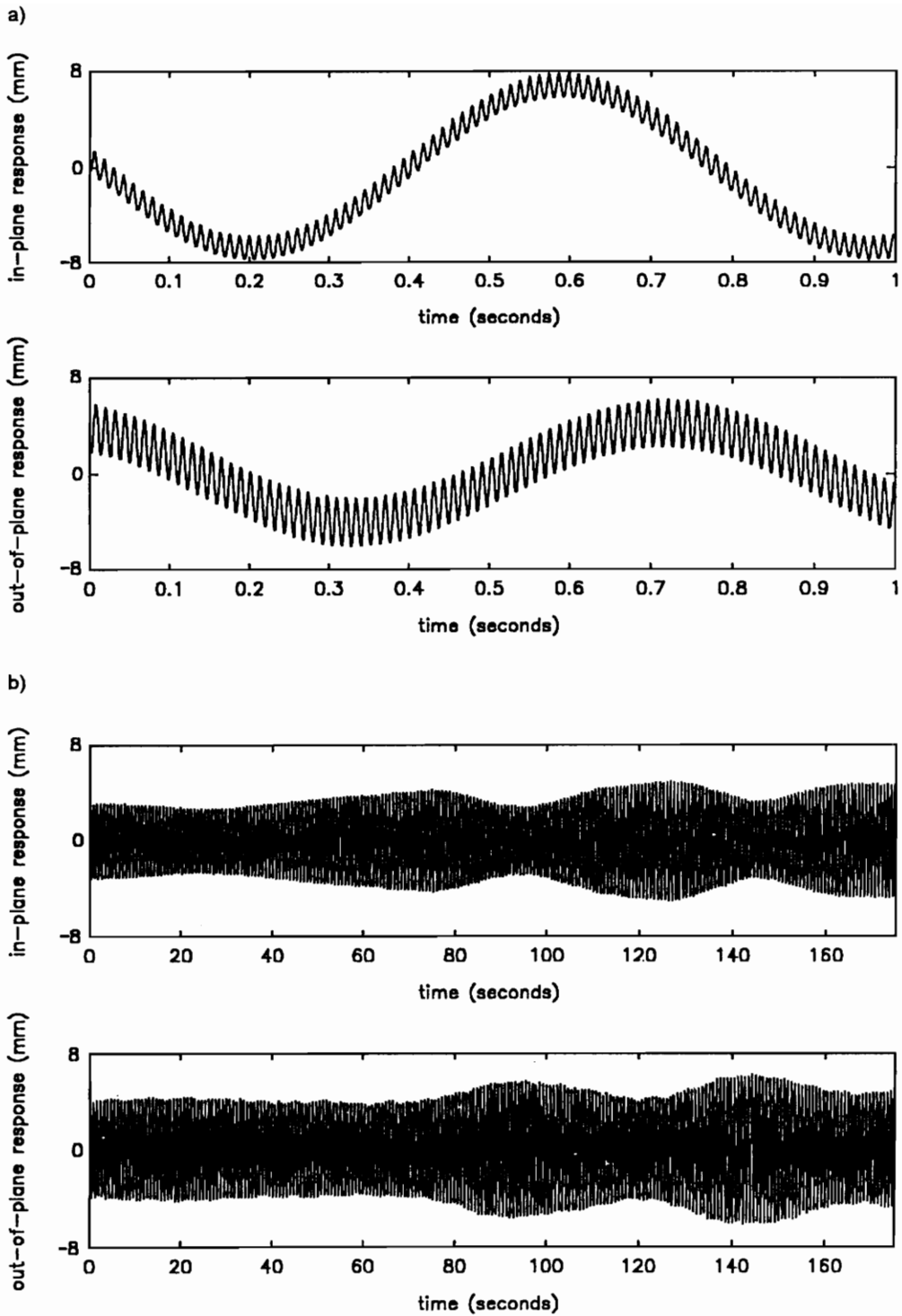
Fig. 2.3 One-second (a) and 170-second (b) time traces of a typical weakly modulated motion
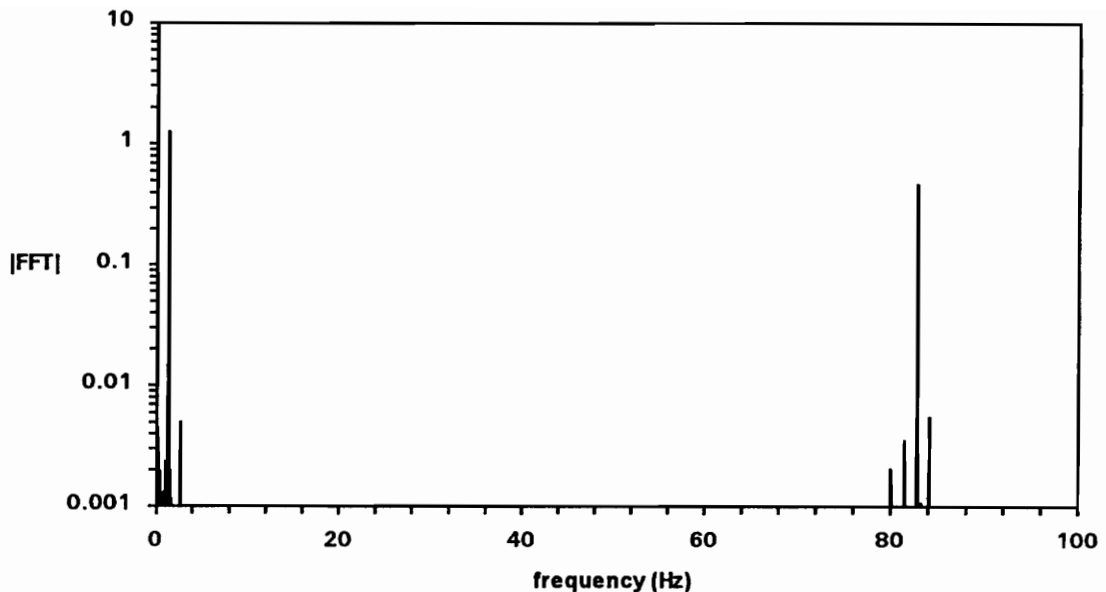
Fig. 2.4   Magnitude of the FFT of a typical weakly modulated motion

larger than that of the directly excited fifth mode.

2.5   Strongly Modulated Motion

As its label implies, the most obvious feature of the strongly modulated motions is
the modulation of the fifth mode. A typical time trace of this type of motion is shown
in Fig. 2.5(a). In contrast to the case of the weakly-modulated motion of Fig. 2.3, the
modulation of the fifth mode is clearly distinguishable without the aid of FFT's. It is
also apparent from the asymmetry in the envelope of the traces shown in Fig. 2.5(a)
that there is a significant low-frequency component present in the response.

In Fig. 2.5(b), a longer time trace of this motion is presented. Here, the scal-
ing of the time axis is such that both the low-frequency component present in the
response and the envelope of the fifth-mode response are clearly discernible. The er-
ratic character of the evolution of the fifth-mode response suggests that the fifth mode
is chaotically modulated. This assertion can be further substantiated by examination

Experiments on a Cantilever Beam   16
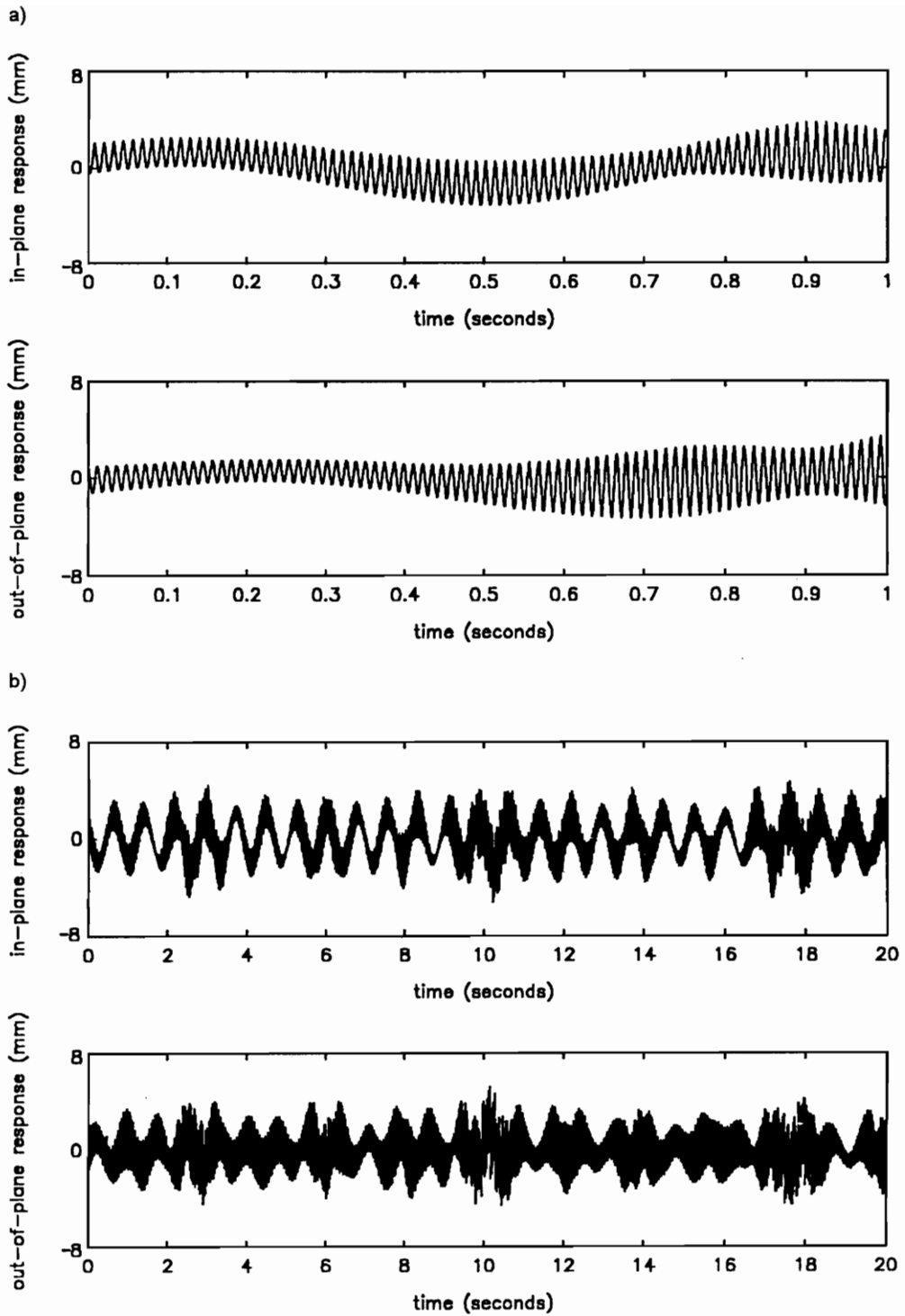
Fig. 2.5 One-second (a) and twenty-second (b) time traces of a typical strongly modulated motion
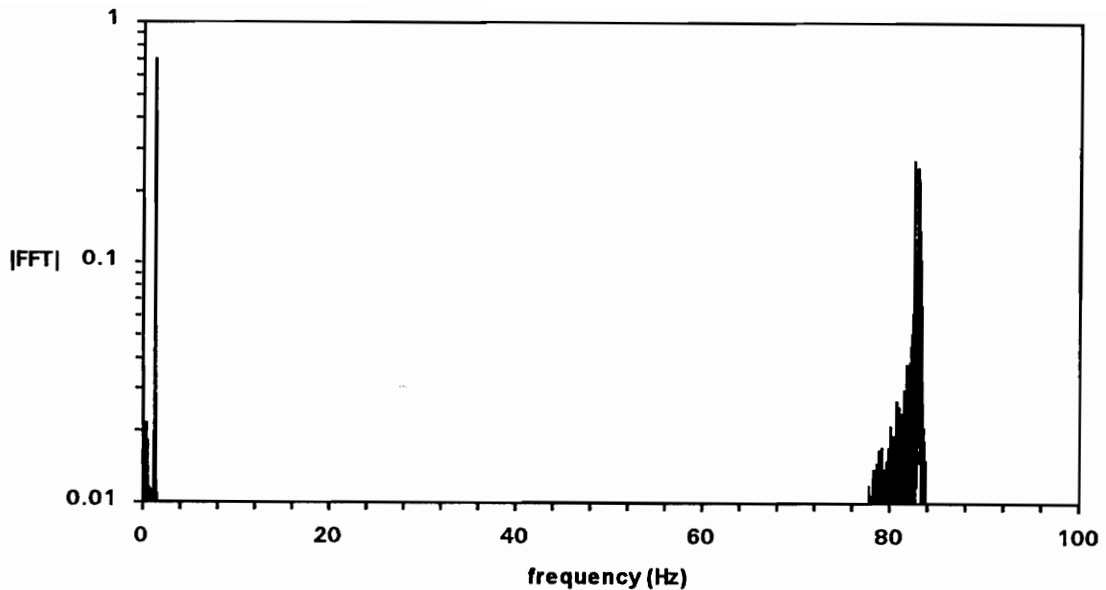
Fig. 2.6   Magnitude of the FFT of a typical strongly modulated motion

of the FFT of this signal shown in Fig. 2.6. The narrow-band response present in the neighborhood of the fifth natural frequency is characteristic of chaotically-modulated motions.

Turning our attention to the low-frequency component present in the response, we find that there is a peak at the first natural frequency of the system and conclude that the low-frequency component in the response is due to the first mode. As in the case of weakly modulated motions, there is a dense set of side bands clustered around the first natural-frequency peak, indicating that the first-mode response is also modulated. Again, due to the slow modulation of the response of the first mode, we are currently unable to obtain an estimate of the amplitude of the first-mode response.

Experiments on a Cantilever Beam   18

2.6   Closure

The results presented here show modal interactions occurring between high- and low-frequency modes in a flexible structure. The mechanism for the interaction appears to be neither a classical internal resonance nor an external or parametric resonance involving the low-frequency modes. Modulations of the amplitudes and phases of the high-frequency modes seem to be essential to the occurrence of these interactions.

Chapter 3

Interaction Between Widely Spaced Modes—Quadratic Nonlinearity

3.1 Introduction

In this chapter, by studying a simple two-degree-of-freedom system with quadratic nonlinearities, we investigate the interaction between widely spaced modes documented in the experiment. We use the method of multiple scales and show that energy can be transferred from high- to low-frequency modes in this simple system. Then we investigate the possibility that energy can be transferred from low- to high-frequency modes and find that this will not generally occur.

3.2 Excitation of the High-Frequency Mode

We consider two coupled oscillators of the form

$$\ddot{u}_1^* + 2\mu_1\omega_1\dot{u}_1^* + \omega_1^2 u_1^* = -\alpha_1 u_2^{*2} \tag{3.1}$$

$$\ddot{u}_2^* + 2\mu_2\omega_2\dot{u}_2^* + \omega_2^2 u_2^* = -2\alpha_2 u_1^* u_2^* + f^* \cos\Omega^* t^* \tag{3.2}$$

where $\omega_1/\omega_2 \ll 1$ and the overdot denotes the derivative with respect to t^*. The high-frequency mode has coordinate u_2^* and the low-frequency mode has coordinate u_1^*. The

20

system has linear viscous damping given by the coefficients μ_1 and μ_2, quadratic non-linearities with the coefficients α_1 and α_2, and an external forcing function $f^* \cos \Omega^* t^*$ which is applied only to the high frequency mode. We wish to investigate the possibility that a large response in the low-frequency mode be generated by an excitation applied to the high-frequency mode near its natural frequency.

3.2.1 Scaling

The first step in the perturbation analysis is to identify the relative sizes of the various terms in the equations. In order to accomplish this, we introduce dimensionless variables given by

$$t = \omega_2 t^*, \; u_1 = u_1^*/c_1, \; u_2 = u_2^*/c_2, \text{ and } \Omega = \Omega^*/\omega_2 \tag{3.3}$$

A natural choice for a small parameter is the ratio of the natural frequencies of the system. We therefore introduce the small dimensionless parameter

$$\epsilon = \frac{\omega_1}{\omega_2} \tag{3.4}$$

Substituting these dimensionless quantities into the equations of motion, we obtain

$$\ddot{u}_1 + 2\mu_1 \epsilon \dot{u}_1 + \epsilon^2 u_1 = -\frac{\alpha_1 c_2^2}{\omega_2^2 c_1} u_2^2 \tag{3.5}$$

$$\ddot{u}_2 + 2\mu_2 \epsilon \dot{u}_2 + u_2 = -\frac{2\alpha_2 c_1}{\omega_2^2} u_1 u_2 + \frac{f^*}{\omega_2^2 c_2} \cos \Omega t \tag{3.6}$$

where the overdot denotes the derivative with respect to t. At this point, we are free to choose values for c_1 and c_2 and we can thereby scale the system so that the nonlinearities appear at any order. It is important to note that completely different results can be obtained for differently ordered problems. If the nonlinearities are placed at too low or too high an order, their effects will be either dominant or insignificant compared to the linear inertia, damping, and excitation terms.

We therefore scale the system so that the effects of the inertia, damping, and excitation appear at the same order. Such a special scaling is often referred to as

a distinguished limit (there may be more than one distinguished limit for any given system). By scaling the system in this manner, we ensure that the effects of all of the terms in the equations are captured in the expansion. Later, assumptions regarding the sizes of the terms appearing in the expansion can be introduced and further approximations can be made.

For this system, a distinguished limit may be obtained by letting

$$c_1 = \frac{\omega_1 \omega_2}{\alpha_2}, \; c_2 = \sqrt{\frac{\omega_1^3 \omega_2}{\alpha_1 \alpha_2}}, \text{ and } f^* = c_2 \omega_1 \omega_2 f \tag{3.7}$$

Under this scaling, the governing equations become

$$\ddot{u}_1 + 2\mu_1 \epsilon \dot{u}_1 + \epsilon^2 u_1 = -\epsilon^2 u_2^2 \tag{3.8}$$

$$\ddot{u}_2 + 2\mu_2 \epsilon \dot{u}_2 + u_2 = -2\epsilon u_1 u_2 + \epsilon f \cos \Omega t \tag{3.9}$$

Physical interpretation of this scaling depends on the magnitudes of the coefficients α_1 and α_2. For example, if both α_1 and α_2 are $O(\omega_2^2)$, $c_1 = O(\epsilon)$ and $c_2 = O(\epsilon^{3/2})$. Consequently, u_1 and u_2 are both 'stretched' variables. In effect, when we expand for $O(1)$ oscillations of u_1 and u_2, we are assuming very small oscillations in the dimensional variables. The expansion will only be valid for small oscillations. If $\alpha_1 = O(\omega_1^2)$ and $\alpha_2 = O(\omega_1 \omega_2)$, both c_1 and c_2 are $O(1)$. In this case, there is no stretching and the expansion will be valid for $O(1)$ oscillations in the dimensional variables.

Finally, we will find it necessary to show explicitly that the excitation frequency is close to the natural frequency of the high-frequency mode (which is now nondimensionalized to unity). We therefore introduce the detuning parameter σ defined by

$$\Omega = 1 + \frac{1}{2}\epsilon\sigma \tag{3.10}$$

3.2.2 Perturbation Analysis

We use the method of multiple scales (Nayfeh, 1981) to determine a first-order expansion for the system response. A novel feature of this analysis is that, whereas the

high-frequency mode evolves on the fast scale and its amplitude and phase evolve on the slow scale, the low-frequency mode evolves on the slow scale. That is, the new independent variables $T_0 = t$, $T_1 = \epsilon t$, and $T_2 = \epsilon^2 t$ characterize, respectively, motions whose frequencies are near the frequency of the high-frequency mode, the low-frequency mode, and lower frequencies. Using the chain rule, we rewrite the total time derivative in terms of the T_i as

$$\frac{d}{dt} = D_0 + \epsilon D_1 + \epsilon^2 D_2 + \dots \tag{3.11}$$

where $D_n = \partial/\partial T_n$. We assume expansions for the u_i of the form

$$u_i(t) = u_{i0}(T_0, T_1, T_2, \dots) + \epsilon u_{i1}(T_0, T_1, T_2, \dots) + \epsilon^2 u_{i2}(T_0, T_1, T_2, \dots) + \dots \tag{3.12}$$

Substituting Eqs. (3.11) and (3.12) into Eqs. (3.8) and (3.9) and equating the coefficients of equal powers of ϵ, we obtain

$$D_0^2 u_{10} = 0 \tag{3.13}$$

$$D_0^2 u_{11} = -2D_0(D_1 u_{10} + \mu_1 u_{10}) \tag{3.14}$$

$$D_0^2 u_{12} = -(D_1^2 + 2D_0 D_2)u_{10} - 2D_0 D_1 u_{11} - 2\mu_1(D_1 u_{10} + D_0 u_{11}) \tag{3.15}$$
$$-u_{10} - u_{20}^2$$

and

$$D_0^2 u_{20} + u_{20} = 0 \tag{3.16}$$

$$D_0^2 u_{21} + u_{21} = -2D_0(D_1 u_{20} + \mu_2 u_{20}) - 2u_{10}u_{20} + f \cos \Omega t \tag{3.17}$$

$$D_0^2 u_{22} + u_{22} = -(D_1^2 + 2D_0 D_2)u_{20} - 2\mu_2(D_1 u_{20} + D_0 u_{21}) \tag{3.18}$$
$$+2u_{10}u_{21} + 2u_{11}u_{20}$$

Here, we note that Eqs. (3.13)–(3.15) are not in the form of oscillators; this is because the linear restoring force appears at second order in Eq. (3.8).

The solutions to the leading-order problems, Eqs. (3.13) and (3.16), can be written as

$$u_{10} = A(T_1, T_2) + C(T_1, T_2)T_0 \tag{3.19}$$

$$u_{20} = B(T_1, T_2)e^{iT_0} + \bar{B}(T_1, T_2)e^{-iT_0} \qquad (3.20)$$

We require that the response be free of secular terms and therefore set $C = 0$. It follows from Eqs. (3.19) and (3.20) that, in the approximation, u_{10} is a slowly varying function and u_{20} consists of a slowly varying complex amplitude on a rapidly varying carrier.

Next, by eliminating secular terms from the $O(\epsilon)$ problem, we determine an equation governing the slowly varying complex amplitude B. Substitution of Eqs. (3.20) and (3.19) into Eq. (3.17) yields

$$D_0^2 u_{21} + u_{21} = \left(-2iB' - 2i\mu_2 B - 2BA + \frac{1}{2}fe^{i\sigma T_1/2}\right)e^{iT_0} + cc \qquad (3.21)$$

where the prime indicates partial-differentiation with respect to T_1 and cc denotes the complex conjugate of the preceding terms. Secular terms are those that cause u_{21} to grow without bound as $T_0 \to \infty$. In this equation, the secular terms are the terms whose time dependence is of the form e^{iT_0}. We set them equal to zero to obtain the averaged or modulation equation governing B:

$$-2iB' - 2i\mu_2 B - 2BA + \frac{1}{2}fe^{i\sigma T_1/2} = 0 \qquad (3.22)$$

This approximation can be refined by eliminating secular terms from the higher-order problem given by Eq. (3.18) but for the purposes of this study we stop here.

We now write B in terms of the real variables for the amplitude a and phase β as

$$B = \frac{1}{2}ae^{i(\sigma T_1/2 + \beta)} \qquad (3.23)$$

Substituting this expression into the modulation equation governing B and separating the result into real and imaginary parts, we obtain

$$a' = -\left(\mu_2 a + \frac{1}{2}f\sin\beta\right) \qquad (3.24)$$

$$a\beta' = -\left[\left(\frac{1}{2}\sigma - A\right)a + \frac{1}{2}f\cos\beta\right] \qquad (3.25)$$

The expansion for u_2 may be written in terms of a and β as

$$u_2 = a\cos(\Omega t + \beta) + \dots \qquad (3.26)$$

Next, we turn to the low-frequency mode and determine an equation governing A. Substituting the leading-order solution given by Eq. (3.19) into the $O(\epsilon)$ problem given by Eq. (3.14), we find that

$$D_0^2 u_{11} = 0 \qquad (3.27)$$

Because the solution for u_{11} has the same form as A, we do not need to include it in our expansion and therefore we set $u_{11} = 0$. We note that no secular terms appear at this order and therefore no information about A can be obtained.

We now substitute the leading-order solutions, Eqs. (3.19) and (3.20), into the $O(\epsilon^2)$ problem given by Eq. (3.15) and obtain

$$D_0^2 u_{12} = -\left[D_1^2 A + 2\mu_1 D_1 A + A + \frac{1}{4}a^2 \left(e^{i(T_0 + \sigma T_1/2 + \beta)} + cc \right)^2 \right] \qquad (3.28)$$

In this case, the secular terms are the slowly varying terms (terms that are functions of only the slow time scales). Elimination of these terms yields the following averaged equation governing A:

$$A'' + 2\mu_1 A' + A + \frac{1}{2}a^2 = 0 \qquad (3.29)$$

Thus, we see that the square of the amplitude of the high-frequency mode appears as an inhomogeneous term in the averaged equation for the low-frequency mode. Therefore, if the amplitude a of the high-frequency mode is constant, a nonzero static deflection will occur in the low-frequency mode. If the high-frequency mode undergoes modulated motion, a will be a function of time and oscillations in the low-frequency mode will be excited as was observed in the experiments.

We now introduce the variables

$$x = A \text{ and } y = A' \qquad (3.30)$$

and write Eq. (3.29) in the first-order form

$$x' = y \qquad (3.31)$$

$$y' = -\left(x + 2\mu_1 y + \frac{1}{2}a^2 \right) \qquad (3.32)$$

The expansion for u_1 is given by

$$u_1 = x + \ldots \tag{3.33}$$

We will use Eqs. (3.31) and (3.32) along with Eqs. (3.24) and (3.25) to study the dynamics of the system.

3.2.3 Fixed Points of the Averaged Equations

The averaged equations, Eqs. (3.31), (3.32), (3.24), and (3.25), can be used to study the transient as well as the long-time behavior of the system. In this study, we are interested in sustained excitation of the low-frequency mode via nonlinear interaction so we focus on the long-time behavior of the system.

Much insight into the long-time (as well as the transient) dynamics of the system can be gained by studying the fixed points or constant solutions of the averaged equations. If a fixed point is stable, we expect that any motion with initial conditions in its neighborhood will eventually settle to it, resulting in constant-amplitude-and-phase motion of the high-frequency mode accompanied by static deflections of the low-frequency mode.

If a fixed point is unstable, trajectories with initial conditions in its neighborhood may either diverge from the fixed point or oscillate about it, depending on the nature of the instability. If the fixed point is a saddle, trajectories will diverge from it and therefore the fixed point does not represent an experimentally attainable state of the system. If the fixed point is an unstable focus, motions are expected to oscillate about it, resulting in modulated motions of the high-frequency mode accompanied by oscillations of the low-frequency mode as observed in the experiments.

Setting the time derivatives equal to zero in Eqs. (3.31), (3.32), (3.24), and (3.25) yields the fixed points of the averaged equations. We find it convenient to solve for σ, x, and β in terms of a to obtain

$$\sigma = -a^2 \pm \sqrt{\frac{f^2}{a^2} - 4\mu_2^2} \tag{3.34}$$

$$x = -\frac{1}{2}a^2 \tag{3.35}$$

$$\beta = \tan^{-1}\left(\frac{2\mu_2}{\sigma + a^2}\right) \tag{3.36}$$

It is clear that the maximum constant amplitude a is $f/2\mu_2$ and, in correspondence, the largest magnitude static deflection x is $-f^2/8\mu_2^2$.

The stability of a fixed point can be ascertained from the eigenvalues of the Jacobian matrix of the averaged equations. Forming the Jacobian matrix, J, by differentiating each of the expressions for x', y', a', and β' by x, y, a, and β in that order and evaluating at the fixed point, we obtain

$$J = - \begin{bmatrix} 0 & -1 & 0 & 0 \\ 1 & 2\mu_1 & a & 0 \\ 0 & 0 & \mu_2 & -q \\ -1 & 0 & q/a^2 & \mu_2 \end{bmatrix} \tag{3.37}$$

where

$$q = \mp\frac{1}{2}a\sqrt{\frac{f^2}{a^2} - 4\mu_2^2} \tag{3.38}$$

We determine the eigenvalues numerically. If the real parts of all of the eigenvalues are negative, the fixed point is stable. The fixed point may lose stability by a real eigenvalue crossing into the right half plane; in this case a saddle is formed. Alternatively, a complex-conjugate pair of eigenvalues may cross transversely into the right half plane; in this case an unstable focus is formed (Guckenheimer and Holmes, 1983). The latter phenomenon is referred to as a Hopf bifurcation and is of primary interest in this study because it indicates that oscillatory motions of x, y, a, and β will occur.

By using Eqs. (3.34) and (3.35) to evaluate σ and x for given values of a, we generate frequency-response curves. We plot heavy lines for stable fixed points and light lines for saddles. At each unstable focus, we integrate the averaged equations and determine the minimum and maximum values of x and a. These are indicated by the vertical lines on the plots. In Fig. 3.1, we present the frequency-response curves
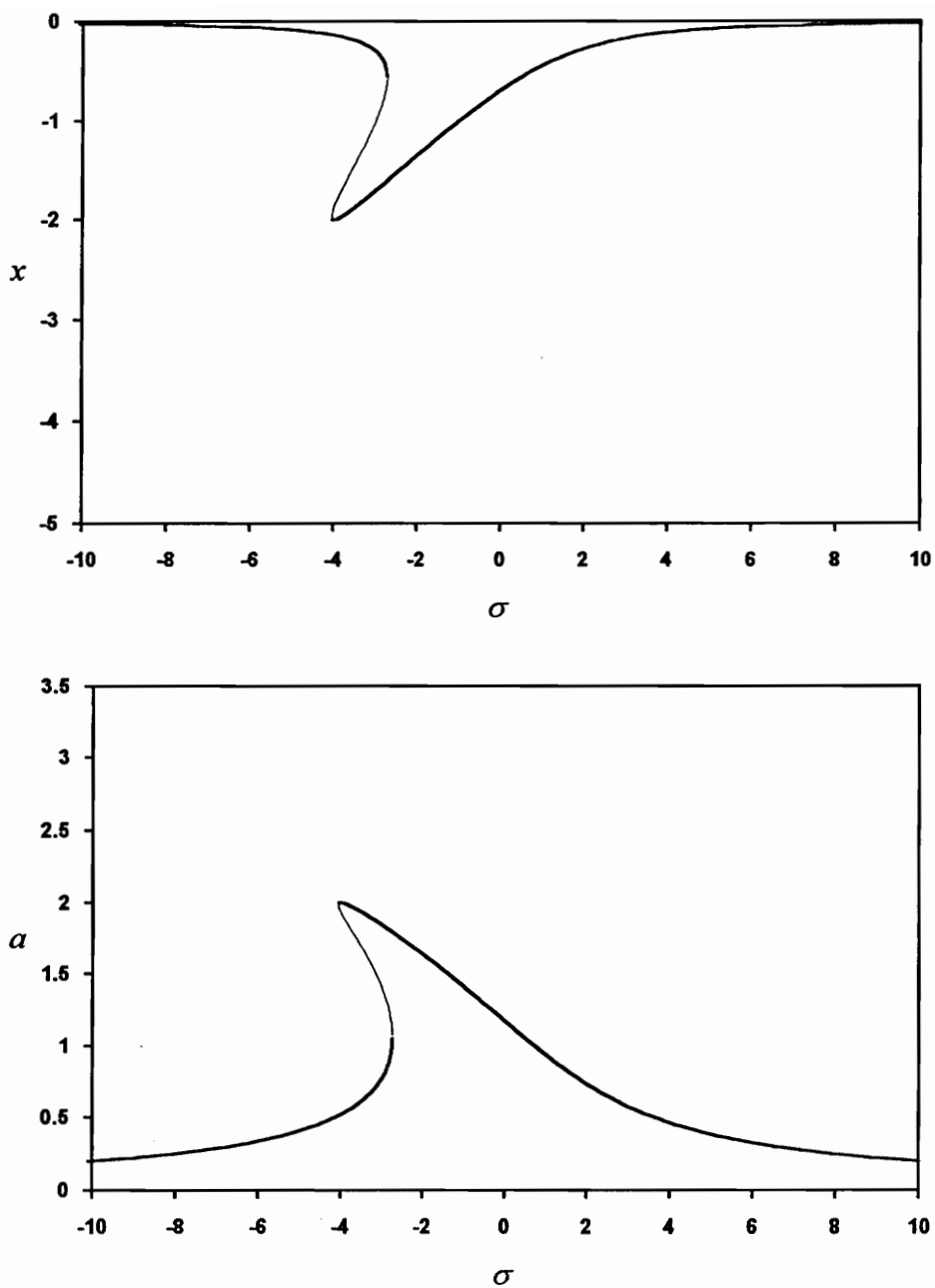
Fig. 3.1   Frequency-response curves for $f = 2.0$, $\mu_1 = 1.0$, and $\mu_2 = 0.5$

for $f = 2.0$, $\mu_1 = 1.0$, and $\mu_2 = 0.5$. For these parameter values, no Hopf bifurcations occur and therefore no oscillatory motions of x are predicted.

Increasing the excitation amplitude f to 3.0, we obtain the frequency-response curves shown in Fig. 3.2. In this case, a Hopf bifurcation occurs giving rise to a branch of unstable foci. Around the unstable foci, oscillatory motions occur with amplitudes indicated by the vertical lines. Thus, sustained oscillations of the low-frequency mode accompanied by amplitude-and-phase-modulated motions of the high-frequency mode occur in this region.

3.2.4 Numerical Integration

In this section, by numerically integrating the averaged equations, we study motion in the neighborhood of the unstable foci. In addition, in order to validate the perturbation analysis, we numerically integrate the full equations and compare the results with those obtained from the averaged equations.

To facilitate numerical integration of the full equations, we write them in a first-order form through the transformations

$$u_1 = x \tag{3.39}$$

$$\dot{u}_1 = \epsilon y \tag{3.40}$$

$$u_2 = a(t)\cos\left(\Omega t + \beta(t)\right) \tag{3.41}$$

$$\dot{u}_2 = -a(t)\Omega\sin\left(\Omega t + \beta(t)\right) \tag{3.42}$$

Substituting these transformations into Eqs. (3.8) and (3.9), we obtain

$$\dot{x} = \epsilon y \tag{3.43}$$

$$\dot{y} = -\epsilon\left(x + 2\mu_1 y + a^2\cos^2\phi\right) \tag{3.44}$$

$$\dot{a} = -\frac{\epsilon g(t)}{\Omega}\sin\phi \tag{3.45}$$

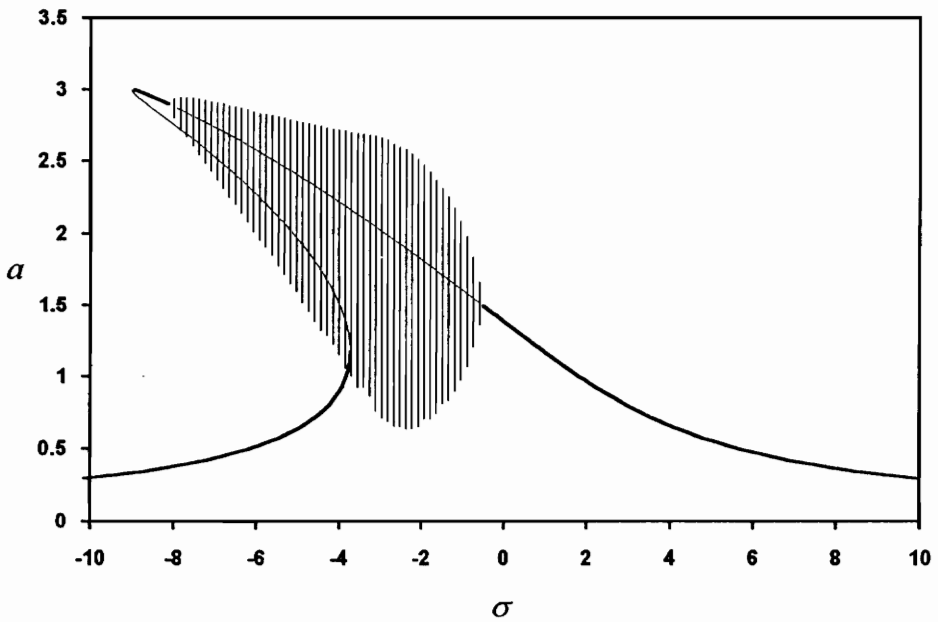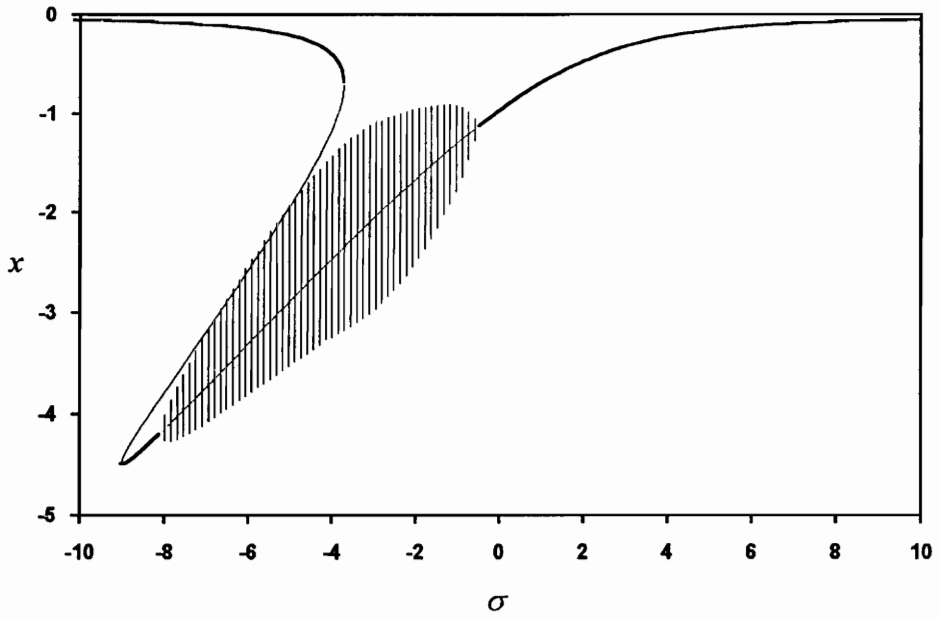$$a\dot{\beta} = -\frac{\epsilon g(t)}{\Omega}\cos\phi \tag{3.46}$$

Fig. 3.2   Frequency-response curves for $f = 3.0$, $\mu_1 = 1.0$, and $\mu_2 = 0.5$

where

$$g(t) = \sigma a \cos \phi - 2ax \cos \phi + 2\mu_2 a\Omega \sin \phi + f \cos \Omega t \qquad (3.47)$$

and

$$\phi = \Omega t + \beta \qquad (3.48)$$

We choose to write the equations in this form because it is less stiff than other forms. Stiffness, caused by the coexistence of slow and fast changes in the system, can be gauged by comparison of the magnitudes of the elements of the Jacobian matrix. Written in terms of the original variables, the system is very stiff and numerical integration is inefficient. However, by introducing x, y, a, and β, we obtain a system whose right-hand side has ϵ as a common factor. Therefore, all terms in the Jacobian are of comparable magnitude, and numerical integration is considerably more efficient than it would be in terms of the original variables.

In the numerical study, we use the same parameter values as in Fig. 3.2. For values of σ between approximately -8.0 and -0.6, unstable foci exist and we therefore expect that oscillatory motions will occur. For values of σ out of this range, we expect that the motion will settle to a fixed point. This was verified for several values of σ outside the range for both the averaged and full equations.

In the region of unstable foci, we integrated the averaged equations at increments of σ as indicated by the spacing of vertical lines in Fig. 3.2. In all cases we found only simple periodic orbits; no multiple solutions or bifurcation phenomena were observed. A sampling of the orbits obtained during this sweep is shown in the left column of Fig. 3.3.

Integrating the full equations for $\epsilon = 0.02$, we obtain results closely matching those obtained from the averaged equations. These orbits are shown in the right column of Fig. 3.3 for comparison with the results obtained from the averaged equations. For values of ϵ as large as 0.10, good qualitative agreement is maintained although quantitative agreement is lost.
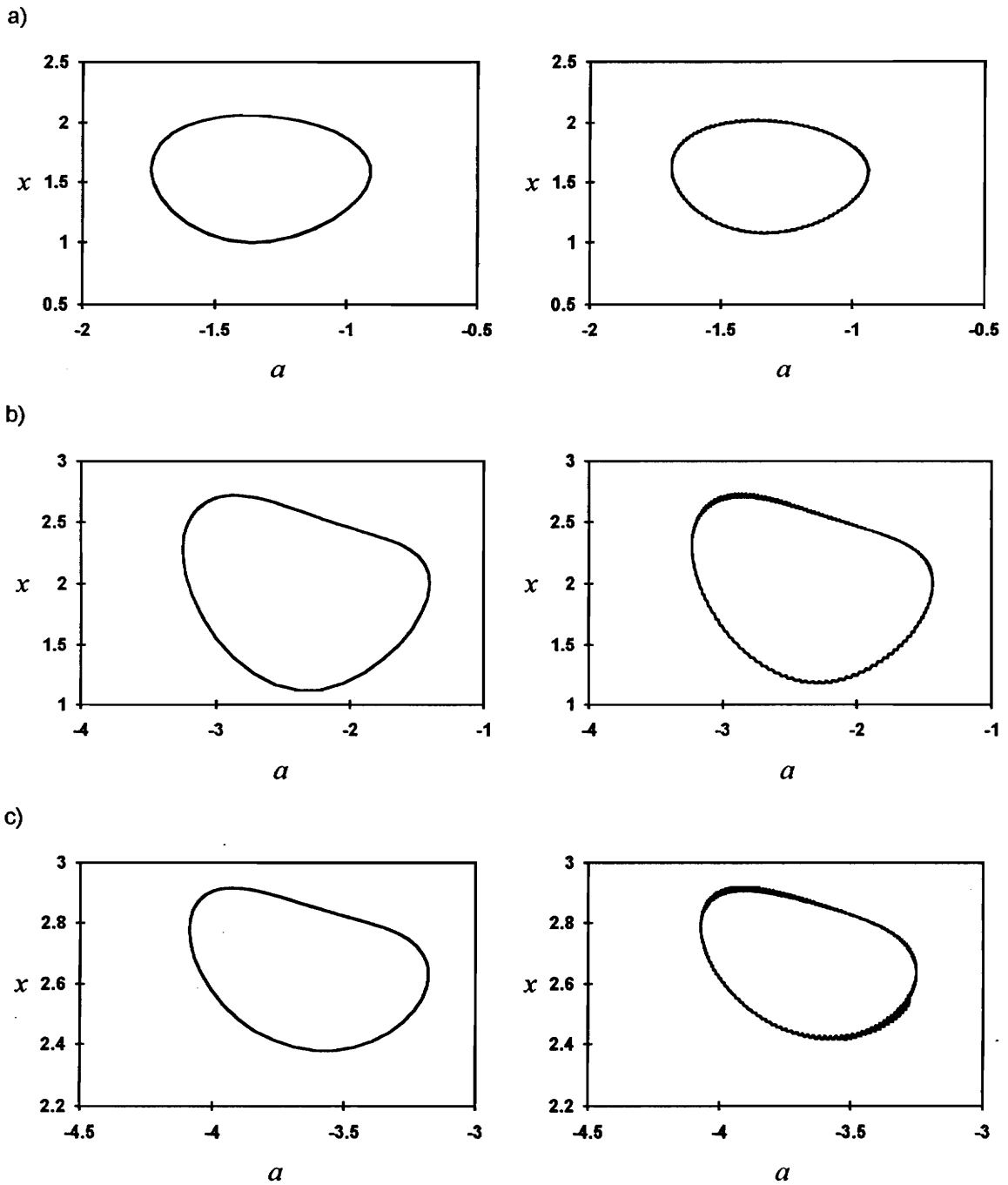
a)

b)

c)

Fig. 3.3   Comparison of the results of numerical integration of the averaged (left) and full (right) equations for $f = 3.0$, $\mu_1 = 1.0$, and $\mu_2 = 0.5$, and σ=(a) -1.0, (b) -4.0, and (c) -7.0

3.3 Excitation of the Low-Frequency Mode

In some applications, it may be useful to transfer energy from a low-frequency mode to a high-frequency mode. In this section, we investigate this possibility. That is, we apply an excitation to the low-frequency mode and determine whether sustained oscillations of the high-frequency mode can occur. We study the system

$$\ddot{u}_1 + 2\mu_1\epsilon\dot{u}_1 + \epsilon^2 u_1 = -\epsilon^2 u_2^2 + \epsilon^2 f \cos \Omega t \tag{3.49}$$

$$\ddot{u}_2 + 2\mu_2\epsilon\dot{u}_2 + u_2 = -2\epsilon u_1 u_2 \tag{3.50}$$

which has the same form as Eqs. (3.8) and (3.9) studied earlier in this chapter with the exception that the excitation is now applied to the low-frequency mode. We take $\Omega \approx \epsilon$ so that the low-frequency mode will be resonantly excited.

Performing an analysis similar to that applied before, we obtain the averaged equation

$$A'' + 2\mu_1 A' + A + 2B\bar{B} = f \cos \Omega t \tag{3.51}$$

for A and

$$2iB' + 2i\mu_2 B - 2AB = 0 \tag{3.52}$$

for B. Substituting the polar form

$$B = \frac{1}{2}ae^{i\beta} \tag{3.53}$$

into Eq. (3.52) and separating the result into real and imaginary parts, we obtain

$$a' = -\mu_2 a \tag{3.54}$$

$$a\beta' = Aa \tag{3.55}$$

It is clear from Eq. (3.54) that a decays to zero as $T_1 \to \infty$. Thus, excitation of the low-frequency mode will not cause an energy transfer to the high-frequency mode. The modes are strongly coupled, but the nature of the coupling is such that oscillations of the low-frequency mode will not excite the high-frequency mode.

Inspecting Eq. (3.52), we see that the low-frequency modal displacement A appears in a product with the complex amplitude B. That this term has a real coefficient indicates that it is in phase with $\dot{\beta}$. In order to drive the high-frequency mode, it must appear in phase with $\dot{a}$. This can be accomplished through a nonlinear damping term as in the system

$$\ddot{u}_1 + 2\mu_1\epsilon\dot{u}_1 + \epsilon^2 u_1 = -\epsilon^2 u_2^2 + \epsilon^2 f \cos\Omega t \qquad (3.56)$$

$$\ddot{u}_2 + 2\mu_2\epsilon\dot{u}_2 + u_2 = -\epsilon u_1\dot{u}_2 \qquad (3.57)$$

whose averaged equations are given by Eq. (3.51) and

$$a' = -(\mu_2 - A)a \qquad (3.58)$$

$$a\beta' = 0 \qquad (3.59)$$

From Eq. (3.51), we conclude that A will be oscillatory. If, as A oscillates, it is positive and exceeds μ_2 in magnitude, a will increase and the high-frequency mode will be excited. Physical interpretation of the coupling in this system is unclear and it is certainly unusual in mechanical systems. By inspection of the full equation given by Eq. (3.57), we see that large negative values of u_1 make the damping of u_2 negative. Thus, we may consider the oscillations of u_2 to be self excited.

Regarding the possibility of energy transfer from low- to high-frequency modes, we note that countless experiments have been performed on the large forced oscillations of the first few modes of continuous systems, but no report of this phenomenon exists in the literature. This indicates that excitation of the high-frequency mode, if possible in structures, occurs only rarely. It may also be noted that the coupling found in Eq. (3.57) is not actually an energy transfer. Rather, the energy which drives u_2 is added to the system through negative damping.

3.4   Closure

In this chapter, we studied a two-degree-of-freedom system with widely spaced frequencies and quadratic nonlinearities. Using the method of multiple scales, we found

that in this system, interactions between the modes may occur by which an excitation applied to the high-frequency mode can cause sustained oscillations of the low-frequency mode. The motion in this regime resembles that observed in the experiments—a low-frequency motion accompanied by high-frequency oscillations modulated at the frequency of the low-frequency motion.

It was shown that although amplitude and phase modulation of the high-frequency mode must occur in order for the low-frequency mode to be excited, the modulation does not occur independently of the low-frequency mode. Rather, the modulation is a result of an instability involving both the high- and low-frequency modes.

We also investigated the possibility that oscillations of the high-frequency mode may be sustained by driving the low-frequency mode. It was found that this could occur through nonlinear damping, but this mechanism is discounted on physical grounds.

CHAPTER 4

Interaction Between Widely Spaced Modes—Cubic Nonlinearity

4.1 Introduction

In this chapter, we analytically investigate the transfer of energy from high- to low-frequency modes by studying a representative system made up of two coupled oscillators given by

$$\ddot{u}_1 + 2\epsilon\mu_1\dot{u}_1 + \epsilon^2 u_1 = -\epsilon^2(4\alpha_1 u_1^3 + \alpha_2 u_1 u_2^2) \tag{4.1}$$

$$\ddot{u}_2 + 2\epsilon\mu_2\dot{u}_2 + u_2 = \epsilon(\alpha_3 u_2^3 + \alpha_4 u_1^2 u_2 + f\cos\Omega t) \tag{4.2}$$

where ϵ, the ratio of the linear natural frequencies of the system, is small. The high-frequency mode, whose undamped linear natural frequency is nondimensionalized to unity, has coordinate u_2 and the low-frequency mode, whose normalized undamped linear natural frequency is ϵ, has coordinate u_1. The system has linear viscous damping given by the coefficients μ_1 and μ_2, cubic nonlinearities with the coefficients α_i, and an external forcing function $f\cos\Omega t$ which is applied only to the high- frequency mode of the system. Of principal interest is whether an excitation applied to the high-frequency mode near its linear natural frequency can, as observed in the experiments, generate a large response in the low-frequency mode.

36

4.2 Averaging

The method of averaging is based on the assumption that small perturbations, such as weak nonlinearities or light damping, cause slow (low-frequency) variations in the response of a system (see Section 1.2). The fast (high-frequency) variations due to the perturbations are assumed to be insignificant. Essentially, the averaging approximation yields a simplified mathematical representation of the dynamics of the system by smoothing away these fast variations. Thus, it is of basic importance that the components that make up the response be correctly classified as either fast or slow.

As discussed in Chapter 1, the method of averaging (as formulated for weakly nonlinear oscillators) breaks down if any of the frequencies are small and therefore can not be used for a low-frequency mode. An alternative strategy for the low-frequency modes can be developed as follows. Neglecting the damping and nonlinearities, one can write the solution to Eq. (4.1) as $u_1 = A_0 \cos(\epsilon t + \phi_0)$. In this solution, u_1 is $O(1)$, $\dot{u}_1$ is $O(\epsilon)$ and $\ddot{u}_1$ is $O(\epsilon^2)$. This leads us to assume that u_1 itself is slowly varying. Because the natural frequency of u_2 is not small, its motion can be treated in the usual way by assuming that its amplitude and phase are slowly varying as described below.

To explicitly show that u_2 is driven near its linear natural frequency, we set $\Omega^2 = 1 + \epsilon\sigma$, where σ is a measure of the closeness of the excitation frequency to the unperturbed natural frequency of u_2. Next, we apply the variation-of-parameters transformation

$$u_2 = a(t) \cos(\Omega t + \beta(t)) \tag{4.3}$$

$$\dot{u}_2 = -a(t)\Omega \sin(\Omega t + \beta(t)) \tag{4.4}$$

to Eqs. (4.1) and (4.2) and obtain

$$\ddot{u}_1 + 2\epsilon\mu_1\dot{u}_1 + \epsilon^2 u_1 = -\epsilon^2(4\alpha_1 u_1^3 + \alpha_2 u_1 a^2 \cos^2(\Omega t + \beta)) \tag{4.5}$$

$$\dot{a}\Omega = -\epsilon g \sin(\Omega t + \beta) \tag{4.6}$$

$$a\dot{\beta}\Omega = -\epsilon g \cos(\Omega t + \beta) \tag{4.7}$$

where

$$g = \sigma a \cos(\Omega t + \beta) + \alpha_3 a^3 \cos^3(\Omega t + \beta) + \alpha_4 u_1^2 a \cos(\Omega t + \beta) \tag{4.8}$$
$$+ 2\mu_2 a \Omega \sin(\Omega t + \beta) + f \cos \Omega t$$

Examining Eqs. (4.6) and (4.7), we note that $\dot{a}$ and $\dot{\beta}$ are $O(\epsilon)$ whereas Ω is $O(1)$ and that therefore a and β are slowly varying. The averaging approximation is achieved by integrating Eqs. (4.5)–(4.7) with respect to time from 0 to $2\pi/\Omega$ while treating the slowly varying quantities a, β, and u_1 as well as their derivatives as constants. The resulting averaged or modulation equations are

$$\ddot{u}_1 + 2\epsilon \mu_1 \dot{u}_1 + \epsilon^2 u_1 = -\epsilon^2 \left(4\alpha_1 u_1^3 + \frac{1}{2}\alpha_2 u_1 a^2 \right) \tag{4.9}$$

and

$$\dot{a} = -\epsilon \left(\mu_2 a + \frac{1}{2} f \sin \beta \right) \tag{4.10}$$

$$\dot{\beta} = -\epsilon \left(\frac{1}{2}\sigma + \frac{1}{2}\alpha_4 u_1^2 + \frac{3}{8}\alpha_3 a^2 + \frac{f}{2a} \cos \beta \right) \tag{4.11}$$

where we have set $\Omega = 1$. Equation (4.9) can be rewritten as a pair of first-order equations as

$$\dot{u}_1 = \epsilon v_1 \tag{4.12}$$

$$\dot{v}_1 = -\epsilon \left(u_1 + 2\mu_1 v_1 + 4\alpha_1 u_1^3 + \frac{1}{2}\alpha_2 u_1 a^2 \right) \tag{4.13}$$

Here, we point out that because ϵ appears as a common factor in the right-hand sides of Eqs. (4.10)–(4.13), the character of the motion does not depend on the value of ϵ. While ϵ must be small for the averaging approximation to be valid, its value only determines the speed at which the motion evolves; the amplitude and stability of the response are independent of its value. In Section 4.5, we will investigate the validity of the averaging approximation for various values of ϵ.

4.3 Fixed Points of the Averaged Equations

The fixed-point solutions of the averaged equations, Eqs. (4.10)–(4.13), represent constant-amplitude-and-phase motions of the high-frequency mode accompanied by static responses of the low-frequency mode. Setting the time derivatives in Eqs. (4.10)–(4.13) equal to zero and solving for σ and u_1 in terms of a, we obtain

$$u_1 = 0 \tag{4.14}$$

or

$$u_1 = \pm\sqrt{-\frac{1 + \alpha_2 a^2/2}{4\alpha_1}} \tag{4.15}$$

and

$$\sigma = -\frac{3}{4}\alpha_3 a^2 - \alpha_4 u_1^2 \pm \sqrt{\frac{f^2}{a^2} - 4\mu_2^2} \tag{4.16}$$

Equations (4.14)–(4.16) are used to generate frequency-response curves by solving for u_1 and σ for given positive values of a less than $f/2\mu_2$. In Fig. 4.1, we present frequency-response curves for a case where α_1 and α_2 are both positive. In this case, the expression under the radical in Eq. (4.15) is always negative and therefore the only real solutions are those with $u_1 = 0$. For some other values of the parameters, nontrivial solutions for u_1 are possible.

If α_1 is negative and α_2 is positive, nontrivial solutions for u_1 will occur for all values of a and any value of f as shown in Fig. 4.2. If α_1 is positive and α_2 is negative, nontrivial solutions for u_1 will occur when

$$f > 2\mu_2 \sqrt{-\frac{2}{\alpha_2}} \tag{4.17}$$

as illustrated in Figs. 4.3 and 4.4. If both α_1 and α_2 are negative, nontrivial solutions for u_1 will occur for values of a less than $\sqrt{-2/\alpha_2}$ and any value of f.

The stability of a fixed-point solution is studied by examination of the eigenvalues

Fig. 4.1   Frequency-response curves for $\alpha_1 = \alpha_3 = 1$, $\alpha_2 = 2$, $\alpha_4 = 3$, $\mu_1 = 0.25$, $\mu_2 = 0.5$,   and $f = 2.5$; solid lines denote stable nodes and dotted lines denote saddles
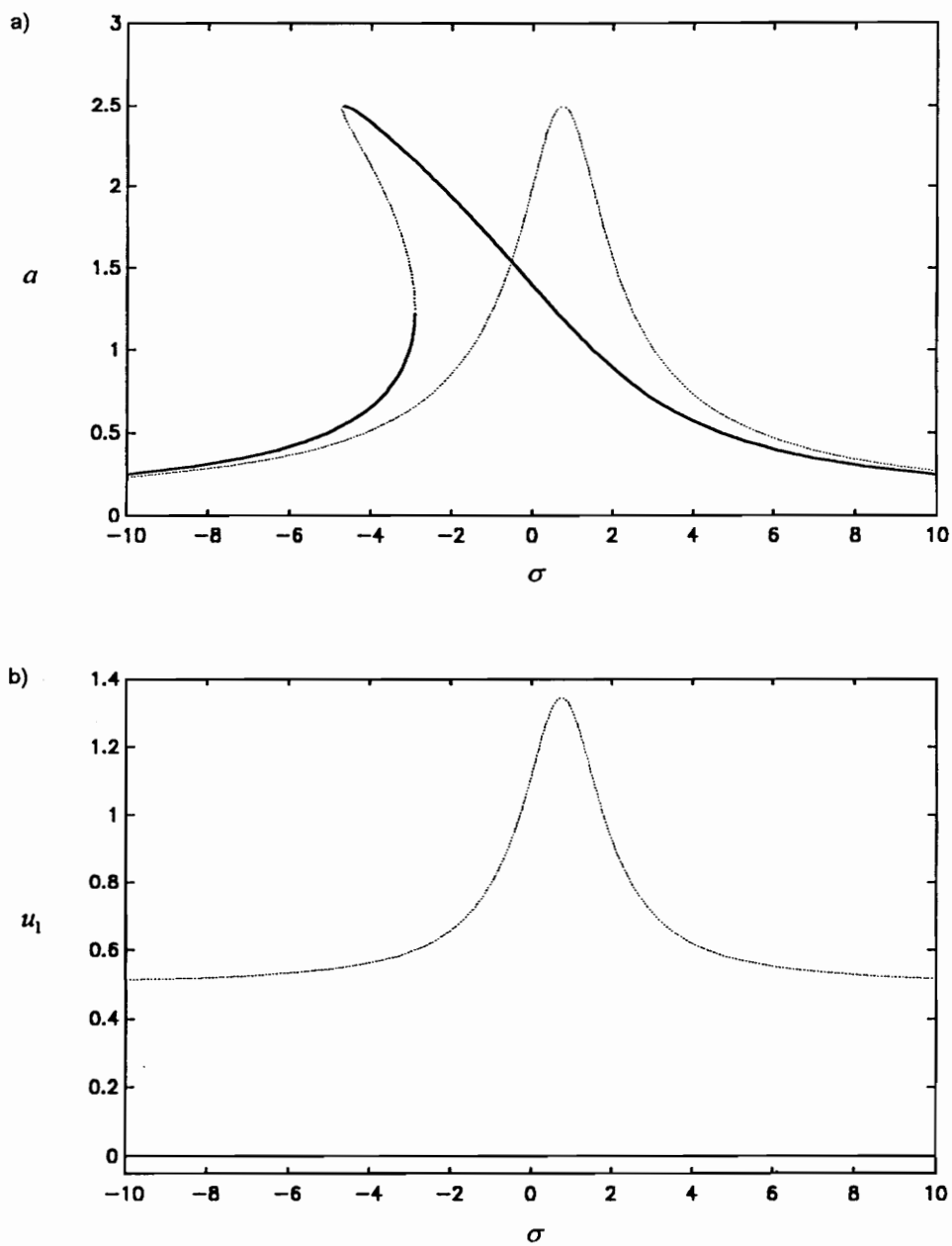
Fig. 4.2 Frequency-response curves for $\alpha_1 = -1$, $\alpha_2 = 2$, $\alpha_3 = 1$, $\alpha_4 = -3$, $\mu_1 = 0.25$, $\mu_2 = 0.5$, and $f = 2.5$; solid lines denote stable nodes and dotted lines denote saddles
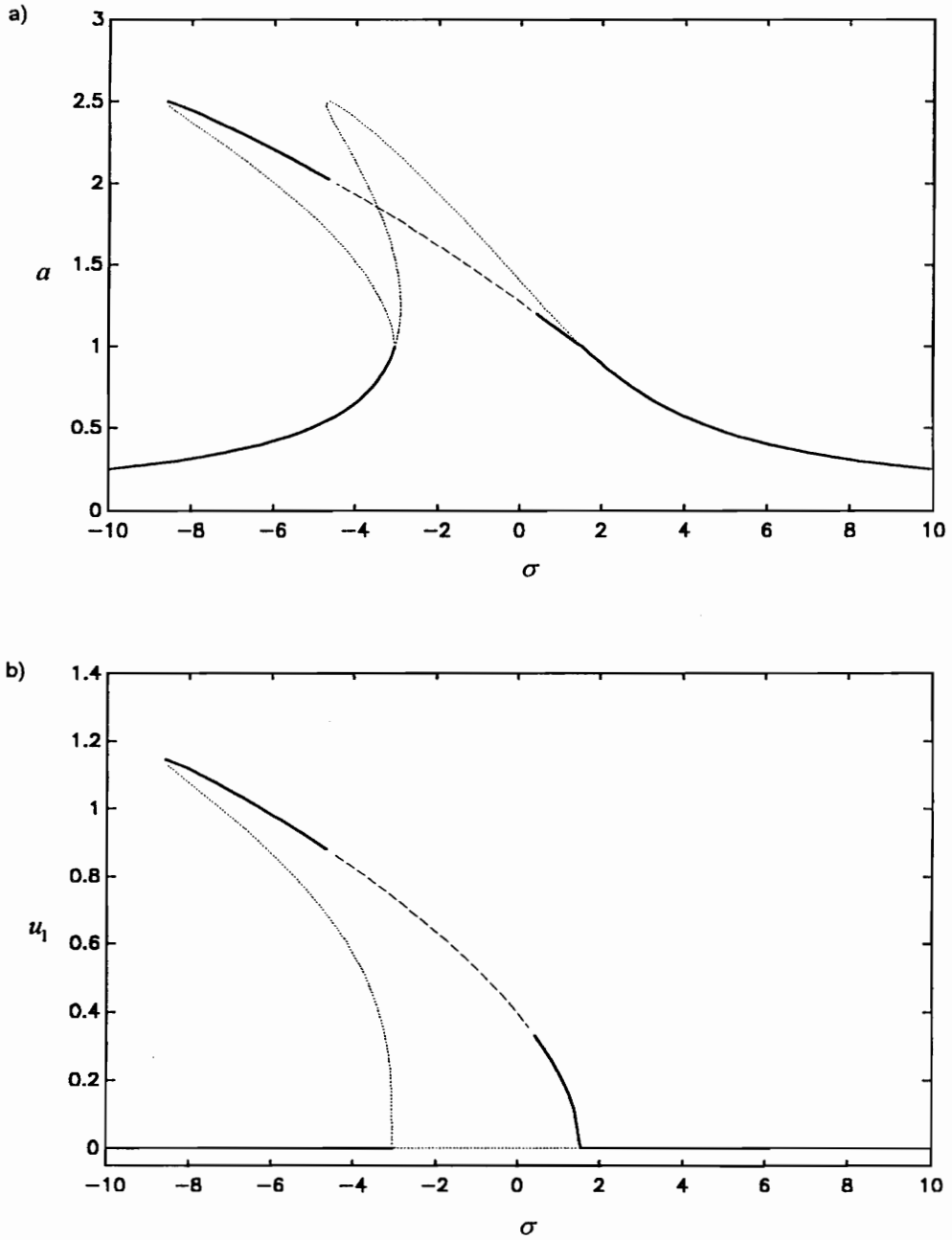
Fig. 4.3 Frequency-response curves for $\alpha_1 = \alpha_3 = 1$, $\alpha_2 = -2$, $\alpha_4 = 3$, $\mu_1 = 0.25$, $\mu_2 = 0.5$, and $f = 2.5$; solid lines denote stable nodes, dotted lines denote saddles, and dashed lines denote unstable foci

a)

b)

Fig. 4.4   Frequency-response curves for $\alpha_1 = \alpha_3 = 1$, $\alpha_2 = -2$, $\alpha_4 = -3$, $\mu_1 = 0.25$, $\mu_2 = 0.5$, and
$f = 2.5$; solid lines denote stable nodes, dotted lines denote saddles, and dashed lines
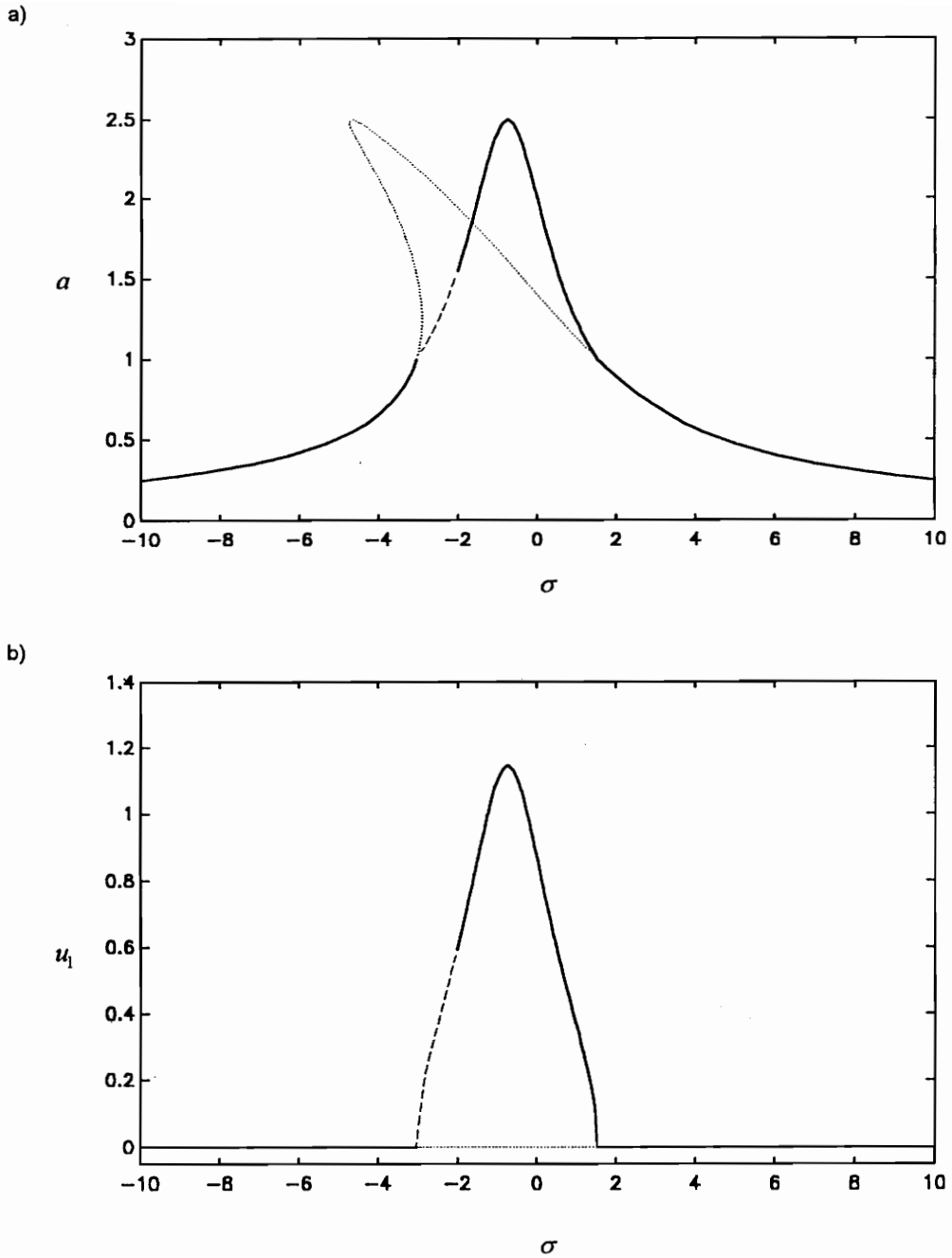denote unstable foci

of the Jacobian matrix of Eqs. (4.10)–(4.13) evaluated at the fixed point of interest:

$$
-\epsilon
\begin{bmatrix}
\mu_2 & \frac{1}{2}f\cos\beta & 0 & 0 \\
\Gamma_1 & \mu_2 & \alpha_4 u_1 & 0 \\
0 & 0 & 0 & -1 \\
\alpha_2 u_1 a & 0 & \Gamma_2 & 2\mu_1
\end{bmatrix}
\tag{4.18}
$$

where

$$
\Gamma_1 = \frac{3}{4}\alpha_3 a - \frac{f}{2a^2}\cos\beta
$$

and

$$
\Gamma_2 = 12a_1 u_1^2 + \frac{1}{2}\alpha_2 a^2 + 1
$$

If all of the eigenvalues have negative real parts, then the fixed point is asymptotically stable and any motion in the neighborhood of this fixed point is expected to settle to it. These solutions are called stable nodes and are denoted by solid lines in the frequency-response curves of Figs. 4.1 through 4.5. If a real eigenvalue becomes positive, the fixed point loses stability and the motion is expected to diverge from it. These unstable solutions are called saddles and are denoted by dotted lines in Figs. 4.1 through 4.4.

If, instead, a Hopf bifurcation occurs by a complex conjugate pair of eigenvalues crossing transversely from the left half of the complex plane into the right half of the complex plane, the fixed point loses stability, but in this case the motion is expected to oscillate about the fixed point. These unstable fixed points (called unstable foci and denoted by dashed lines in Figs. 4.3 and 4.4) are of great interest because in their neighborhood we expect to find motions where u_1 oscillates and u_2 is modulated at the frequency of oscillation of u_1 as observed in the experiments.

For fixed points with $u_1 = 0$, the eigenvalues of the Jacobian matrix are given by

$$
\lambda = -\epsilon\left[\mu_1 \pm \sqrt{\mu_1^2 + \frac{1}{2}\alpha_2 a^2 + 1}\right]
\tag{4.19}
$$

$$
\lambda = -\epsilon\left[\mu_2 \pm \sqrt{f\cos\beta\left(\frac{3}{8}\alpha_3 a - \frac{f}{4a^2}\cos\beta\right)}\right]
\tag{4.20}
$$

Because the damping coefficients μ_1 and μ_2 are always positive, it is clear from Eqs. (4.19) and (4.20) that solutions with $u_1 = 0$ cannot lose stability through a Hopf bifurcation. Therefore we do not expect oscillatory solutions involving u_1 to occur in the neighborhood of fixed points with $u_1 = 0$.

Returning to Fig. 4.1 in which the only possible solutions for u_1 are trivial solutions, we conclude that no Hopf bifurcations can occur for this set of parameters. Thus, in this case and in any case where only trivial fixed-point solutions for u_1 exist, no interactions between u_1 and u_2 can occur and the long-time behavior of the system could be studied using a single-degree-of-freedom equation in which u_1 is neglected.

For fixed points with nontrivial u_1 solutions as given by Eq. (4.15), the eigenvalues cannot be easily obtained in closed form. Instead, we write the equation for the eigenvalues in the form

$$\left(\frac{\lambda}{\epsilon}\right)^4 - r_1 \left(\frac{\lambda}{\epsilon}\right)^3 + r_2 \left(\frac{\lambda}{\epsilon}\right)^2 - r_3 \left(\frac{\lambda}{\epsilon}\right) + r_4 = 0 \qquad (4.21)$$

where

$$r_1 = -2(\mu_1 + \mu_2) \qquad (4.22)$$

$$r_2 = -2 - \alpha_2 a^2 - \frac{3}{8}\alpha_3 a f \cos\beta + \frac{f^2}{4a^2} + 4\mu_1\mu_2 \qquad (4.23)$$

$$r_3 = \frac{3}{4}\mu_1\alpha_3 a f \cos\beta - \frac{\mu_1 f^2}{2a^2} + 4\mu_2 + 2\mu_2\alpha_2 a^2 \qquad (4.24)$$

$$r_4 = \frac{a}{16\alpha_1}(2 + \alpha_2 a^2)(6\alpha_1\alpha_3 - \alpha_2\alpha_4)f\cos\beta - \frac{1}{4}\alpha_2 f^2 - \frac{f^2}{2a^2} \qquad (4.25)$$

Then we use the Routh-Hurwitz criterion to determine the signs of the real parts of the eigenvalues of the Jacobian and therefore the stability of the fixed point. For this case, the Routh-Hurwitz criterion guarantees that all eigenvalues have negative real parts if

$$\begin{aligned}
&i. \qquad r_1 < 0 \\
&ii. \qquad r_1 r_2 - r_3 < 0 \\
&iii. \qquad r_3(r_1 r_2 - r_3) - r_1^2 r_4 > 0 \\
&iv. \qquad r_4 > 0
\end{aligned} \qquad (4.26)$$

We observe that condition i is always satisfied and test the remaining conditions numerically. Of particular interest is the case where condition iii is violated because in this case a complex-conjugate pair of eigenvalues will have a zero or a positive real part and a Hopf bifurcation may occur, resulting in oscillatory motions of u_1.

In Fig. 4.2, we present frequency-response curves for a case in which nontrivial solutions for u_1 occur. It should be noted that, although we show only the positive fixed-point solutions for u_1 in Fig. 4.2(b), there exists a second set of solutions with the opposite sign in u_1. The values of the parameters used in this case differ from those used in Fig. 4.1 only in the signs of α_1 and α_2. The solutions in this case include a set of nontrivial solutions for u_1 in addition to the trivial solutions plotted in Fig. 4.1. This nontrivial branch is, however, unstable with a positive real eigenvalue and therefore does not represent observable states of the system. Because none of the fixed points is an unstable focus, no oscillatory motions of u_1 are predicted for this set of parameters.

By reversing the sign of α_2 used in Fig. 4.1, we obtain the frequency-response curves depicted in Fig. 4.3. In this case, the trivial solutions shown in Fig. 4.1 exist but are unstable with a positive real eigenvalue in the central region of the plot. In this region, a nontrivial solution for u_1 exists. The upper branch of this solution consists of two regions of stable nodes joined by a region of unstable foci. Where the stable nodes exist, the motion will consist of periodic oscillations in u_2 and either a positive or negative static deflection in u_1. Where the unstable foci exist, oscillatory u_1 motions accompanied by modulated u_2 responses will occur.

By reversing the sign of α_4 used in Fig. 4.3, we obtain the frequency-response curves depicted in Fig. 4.4. In this case the nontrivial solutions for u_1 do not exhibit an overhang and occur in a narrower frequency range than in Fig. 4.3. As in the case of Fig. 4.3, there exists a region of unstable foci. Because oscillations in u_1 occur in this region, it is useful to determine its boundaries for a variety of values of the parameters. This can be accomplished by solving for the location of the Hopf

bifurcations which bound the region on each end.

Fixing f, μ_i, and α_i we use the secant method to solve numerically for the values of the frequency detuning σ where condition *iii* is on the verge of being violated. Repeating this procedure for smoothly varying values of f, we obtain curves in the $\sigma - f$ plane which form the boundary between constant-amplitude-and-phase motions of u_2 accompanied by static deflections in u_1 and amplitude-and-phase-modulated motions of u_2 accompanied by oscillations of u_1.

In Fig. 4.5, we present curves generated by this method for the values of the α_i used in Fig. 4.3 and various values of the damping coefficients. Below these curves, oscillations in u_1 decay to a constant value and above them oscillations in u_1 are sustained. From the curves in Fig. 4.5(a), it is apparent that at any particular excitation frequency, increasing the damping coefficient μ_2 of the high-frequency mode increases the critical amplitude of the force required to generate oscillations in u_1. However, from Fig. 4.5(b) we see that increasing the damping coefficient μ_1 of the low-frequency mode does not always increase the critical amplitude of the force. At some excitation amplitudes and frequencies, increasing μ_1 actually destabilizes the system.

For the values of the α_i used in Fig. 4.4, the boundaries between constant and oscillatory motions of u_1 appear as shown in Fig. 4.6. In contrast to the behavior shown in Fig. 4.5, there is in this case a bounded region of values for the forcing amplitude f where instability occurs. That is, at some excitation frequencies, an increase in f will destabilize the system but a further increase in f will re-stabilize it. Also, in Fig. 4.5 an increase in μ_2 never destabilizes the system but in this case an increase in μ_2 may do so.

4.4 Numerical Solutions of the Averaged Equations

In the preceding section, we studied the fixed points of the averaged equations and were able to draw conclusions about motions in their neighborhoods. We can only
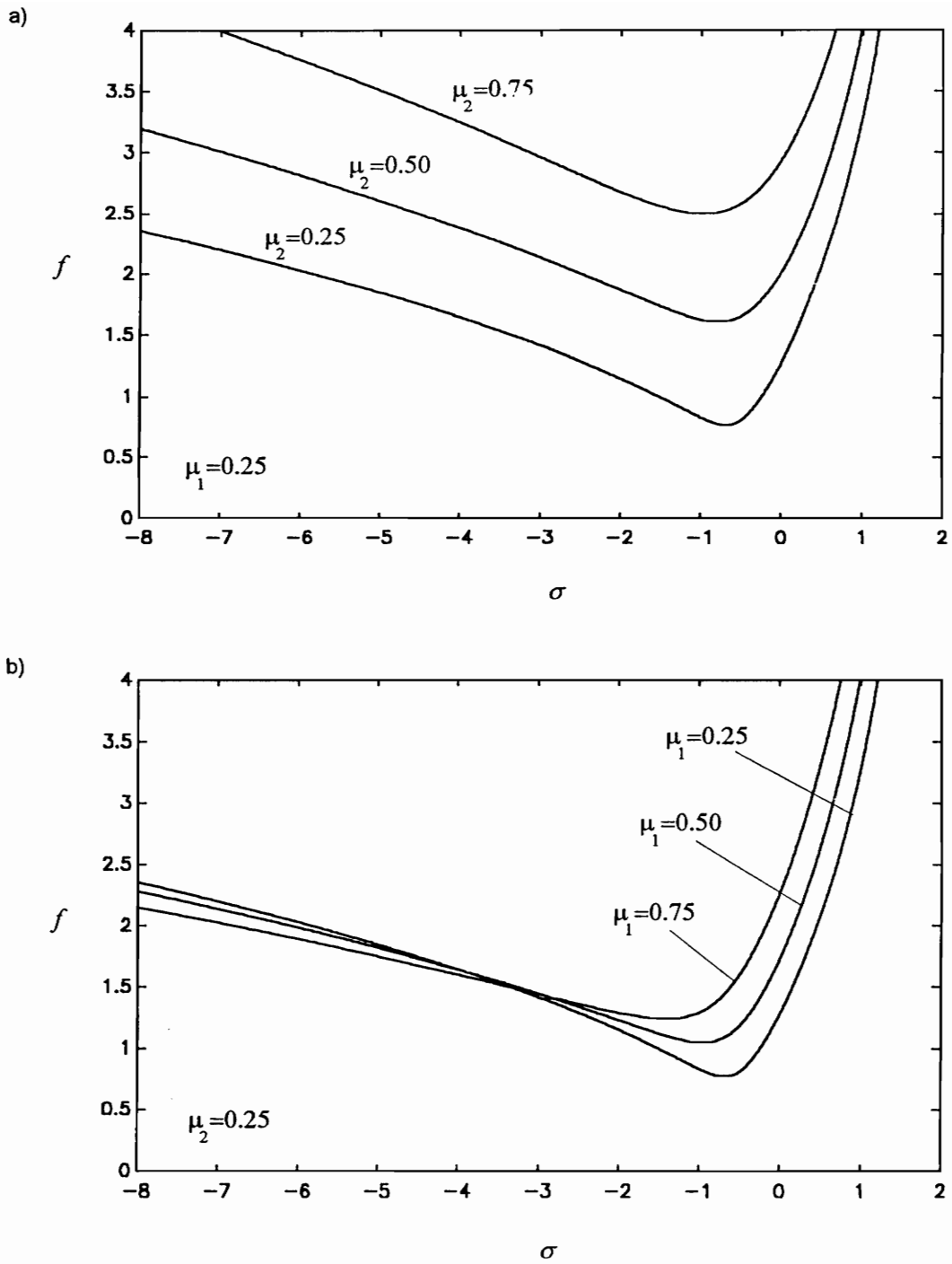
Fig. 4.5 Boundaries between constant and oscillatory motions of u_1 for $\alpha_1 = \alpha_3 = 1$, $\alpha_2 = -2$, $\alpha_4 = 3$, and various damping values
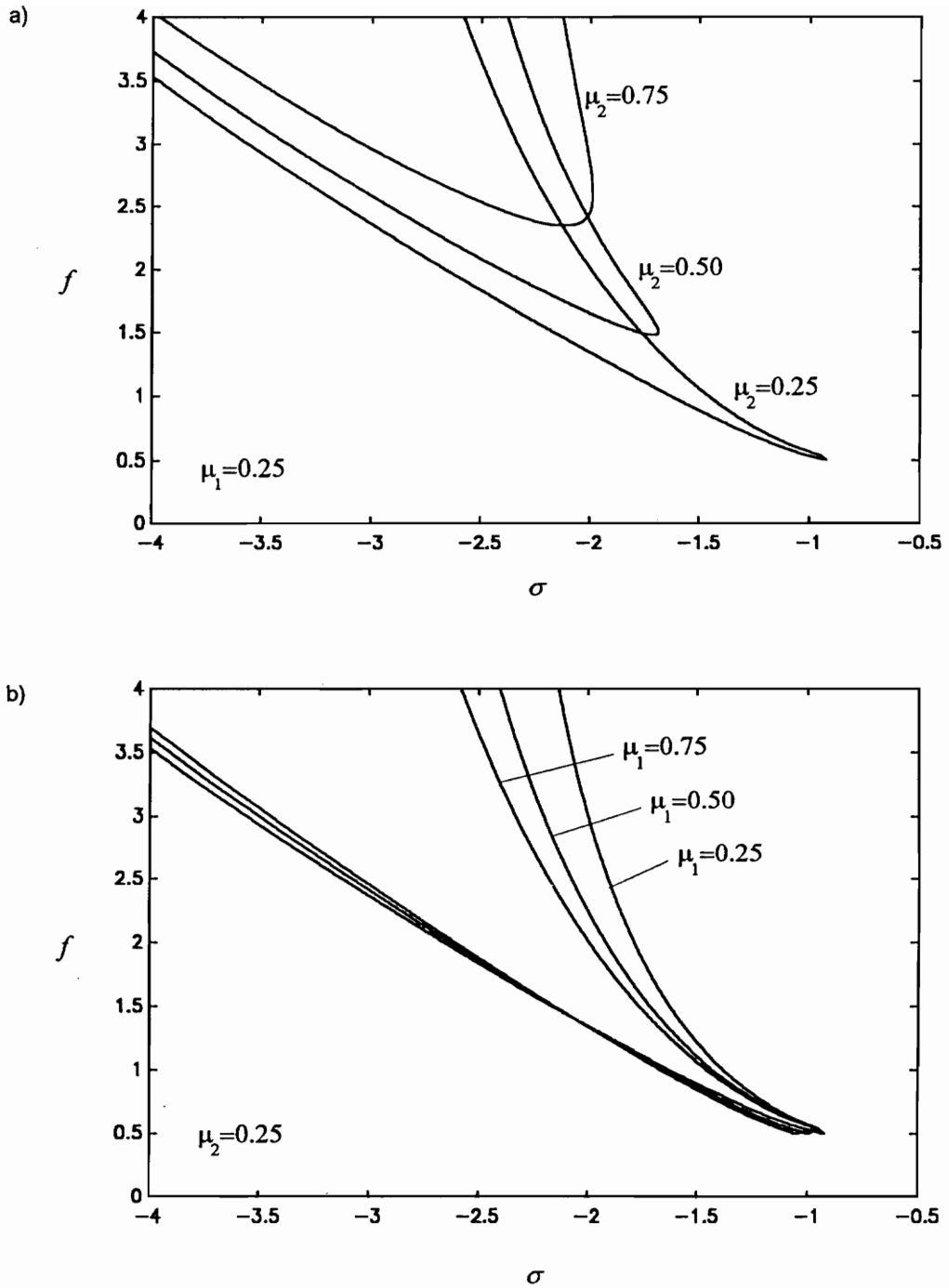
Fig. 4.6 Boundaries between constant and oscillatory motions of u_1 for $\alpha_1 = \alpha_3 = 1$, $\alpha_2 = -2$, $\alpha_4 = -3$, and various damping values

draw conclusions about the general motion of the system if it tends toward these fixed points. While an analytical proof that this is the case does not exist, some confidence that the motion tends toward the fixed points can be obtained by numerically integrating the averaged equations with a variety of initial conditions. We employed a fourth-order Runge-Kutta-Fehlberg algorithm and integrated the averaged equations using the same values for the parameters that were used to make the preceding figures. It was found that, wherever one or more stable fixed points exists, the motion settled to a fixed point for all of the initial conditions that were used.

Next, we study the dynamics of the system in the neighborhoods of unstable foci. As predicted by the stability analysis, oscillatory responses of u_1 are found to occur here. The dynamics of the system are very complicated in these regimes and various nonlinear phenomena, such as sequences of period-doubling bifurcations culminating in chaos, symmetry-breaking bifurcations, the existence of multiple attractors, and the merging of attractors were observed. In this thesis, only a small sample of these dynamics are presented.

In Fig. 4.7, we present a sequence of responses obtained for the same parameters used in Figs. 4.3 and 4.5, $f = 2.5$, and various values of σ. As shown in Fig. 4.3, as σ is decreased through $\sigma = 0.349$, a Hopf bifurcation occurs. In Fig. 4.7(a) we plot the motion in the $a - u_1$ plane just before the Hopf bifurcation occurs. As expected, the long-time response consists of only the stable fixed point. It should be noted that there exists a second fixed-point solution with negative u_1 which is not plotted here.

In Fig. 4.7(b), we show the motion just after the bifurcation. As predicted, the response changes from the point in the plane shown in Fig. 4.7(a) to the limit cycle shown in Fig. 4.7(b). As σ is further decreased, the size of the limit cycle increases as shown in Figs. 4.7(b)–(e). Decreasing σ further, we obtain the period-doubling bifurcation sequence of Figs. 4.7(f)–(g) which culminates in the creation of the chaotic attractor shown in Fig. 4.7(h). It should be noted that only a short sample of the chaotic attractor is shown. As the motion continues, the trajectory will fill the area
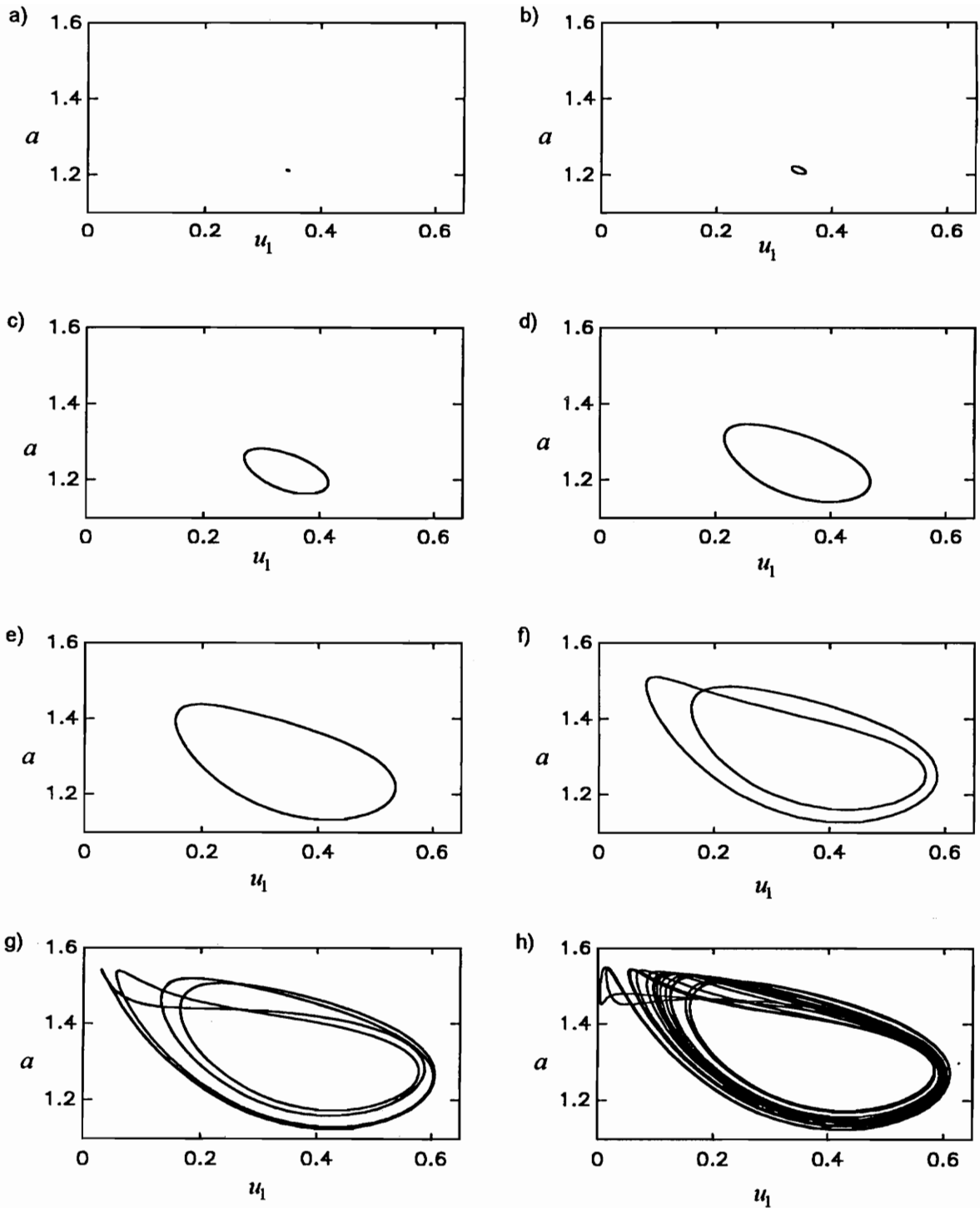
Fig. 4.7 Numerical simulation of the averaged equations for $\alpha_1 = \alpha_3 = 1$, $\alpha_2 = -2$, $\alpha_4 = 3$, $\mu_1 = 0.25$, $\mu_2 = 0.5$, $f = 2.5$, and $\sigma =$ (a) 0.350 , (b) 0.348, (c) 0.300, (d) 0.200, (e) 0.000, (f) -0.170, (g) -0.243, and (h) -0.260

a)

1.6

1.4

a

1.2

−0.5　　0　　0.5

u_1

b)

1.6

1.4

a

1.2

−0.5　　0　　0.5

u_1

c)

1.6

1.4

a

1.2

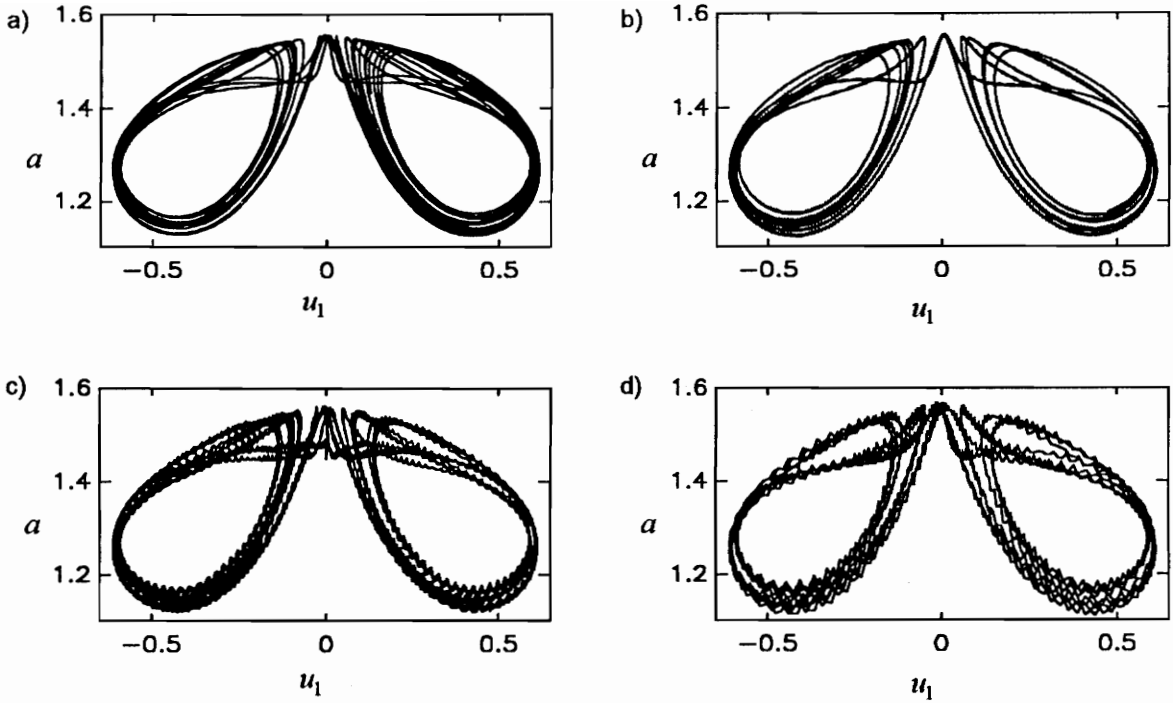−0.5　　0　　0.5

u_1

d)

1.6

1.4

a

1.2

−0.5　　0　　0.5

u_1

Fig. 4.8　Numerical simulation of (a) the averaged equations and (b)-(d) the exact equations for $\alpha_1 = \alpha_3 = 1$, $\alpha_2 = -2$, $\alpha_4 = 3$, $\mu_1 = 0.25$, $\mu_2 = 0.5$, $f = 2.5$, $\sigma = -0.27$, and $\varepsilon =$ (b) 0.01, (c) 0.03, and (d) 0.05

outlined roughly by the portion of the trajectory shown.

For all of the responses shown in Fig. 4.7, there exists a mirror image with opposite signs of u_1 and v_1 in the left half of the plane. Decreasing σ further, the chaotic attractors in the left and right halves of the $a - u_1$ plane merge into a single attractor. That is, the motion does not remain in either the left or right half of the plane but jumps erratically from one to the other. This response is shown in Fig. 4.8(a). As σ is further decreased through roughly -0.41, this attractor loses stability. The motion is no longer attracted to it but rather diverges from it after some time and jumps to another attractor (depicted in Fig. 4.9(a)) which, for values of σ less than roughly -0.2, coexists with the attractors discussed thus far.

As shown in Fig. 4.9(a) this attractor is periodic and symmetric at $\sigma = -0.41$.

As σ is decreased, a symmetry-breaking bifurcation occurs; one of the two resulting nonsymmetric attractors is shown in Fig. 4.9(b). As σ is further decreased, these attractors undergo a sequence of period-doubling bifurcations leading to chaos as shown in Figs. 4.9(c)–(e). The chaotic attractor in Fig. 4.9(e) is unsymmetric and an attractor with its mirror image also exists. Another decrease in σ causes these attractors to merge, resulting in the symmetric attractor shown in Fig. 4.9(f). As σ is further decreased, a great variety of nonlinear dynamical phenomena are observed until a reverse Hopf bifurcation occurs at the end of the unstable branch leading to stable fixed-point solutions.

4.5 Numerical Solutions of the Exact Equations

To confirm the analytical results, we numerically integrate the equations of motion. However, rather than integrate the equations in terms of the original variables u_1 and u_2 as given in Eqs. (4.1) and (4.2), we employ the variables u_1, a, and β as in Eqs. (4.5)–(4.7). This form of the equations, while still exact, is less stiff than Eqs. (4.1) and (4.2) and allows direct comparison to the results obtained from the averaged equations.

In Fig. 4.10, we present results for the same values of the parameters used in Fig. 4.7 with $\epsilon = 0.01$. Comparing Figs. 4.7(a)–(b) and 4.10(a)–(b), we conclude that the averaging approximation predicts the occurrence of the Hopf bifurcation with good accuracy for this value of ϵ. Also, following the evolution of the attractor through the sequence of period-doubling bifurcations to the formation of the chaotic attractor, we find remarkably good agreement as shown in Figs. 4.10(c)–(h). In addition, the averaged and exact equations are in good agreement in the prediction of the merged attractors of Fig. 4.8 for values of ϵ as large as 0.05.

For the less robust attractors, such as the period-two, period-four, and chaotic attractors of Figs. 4.7(f)–(h), the agreement between the averaged and exact equations breaks down for larger values of ϵ. For example, the period-four response predicted
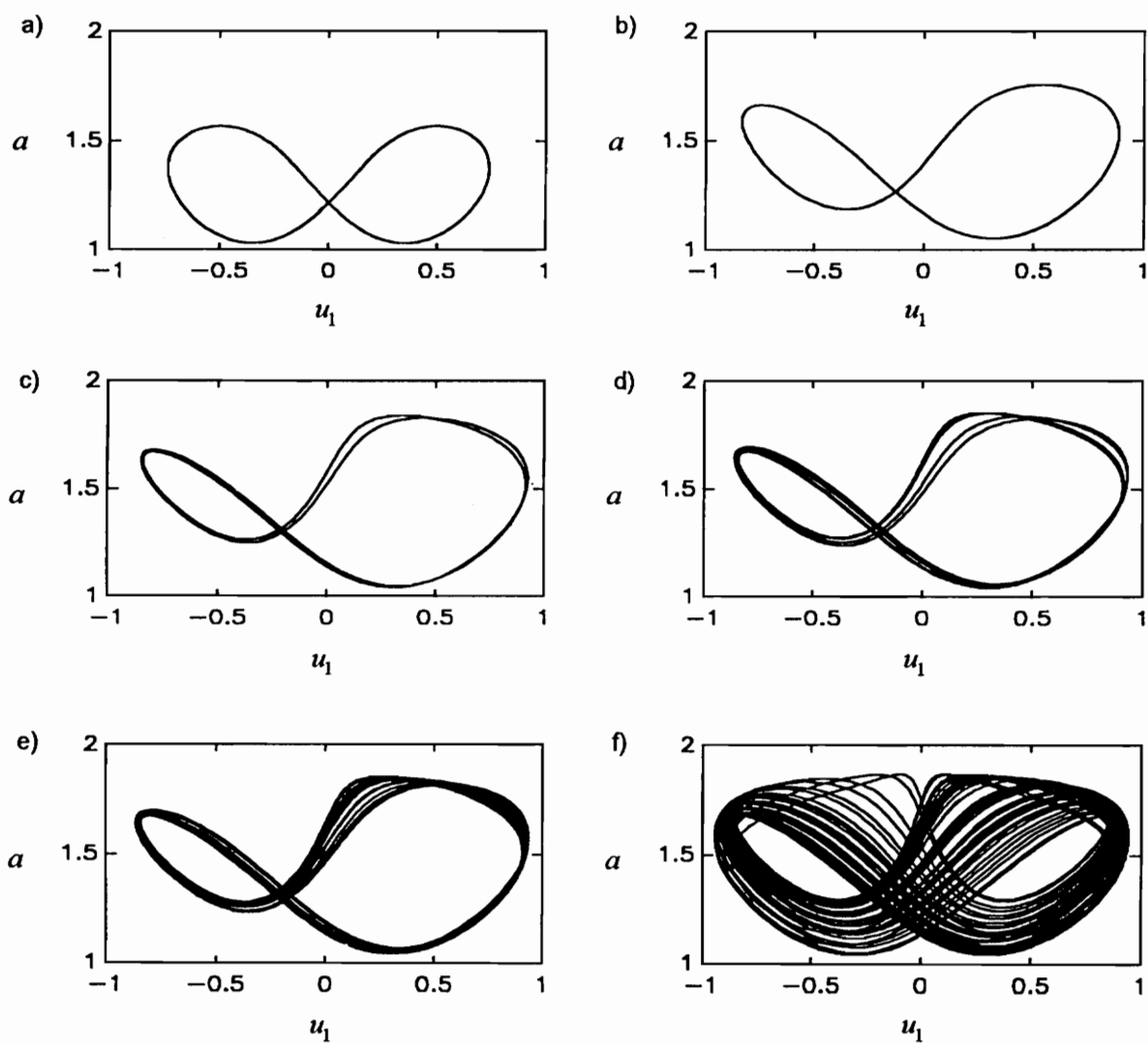
Fig. 4.9   Numerical simulation of the averaged equations for $\alpha_1 = \alpha_3 = 1$, $\alpha_2 = -2$, $\alpha_4 = 3$, $\mu_1 = 0.25$, $\mu_2 = 0.5$, $f = 2.5$, and $\sigma = $ (a) -0.41, (b) -1.10, (c) -1.28, (d) -1.31, (e) -1.32, and (f) -1.36
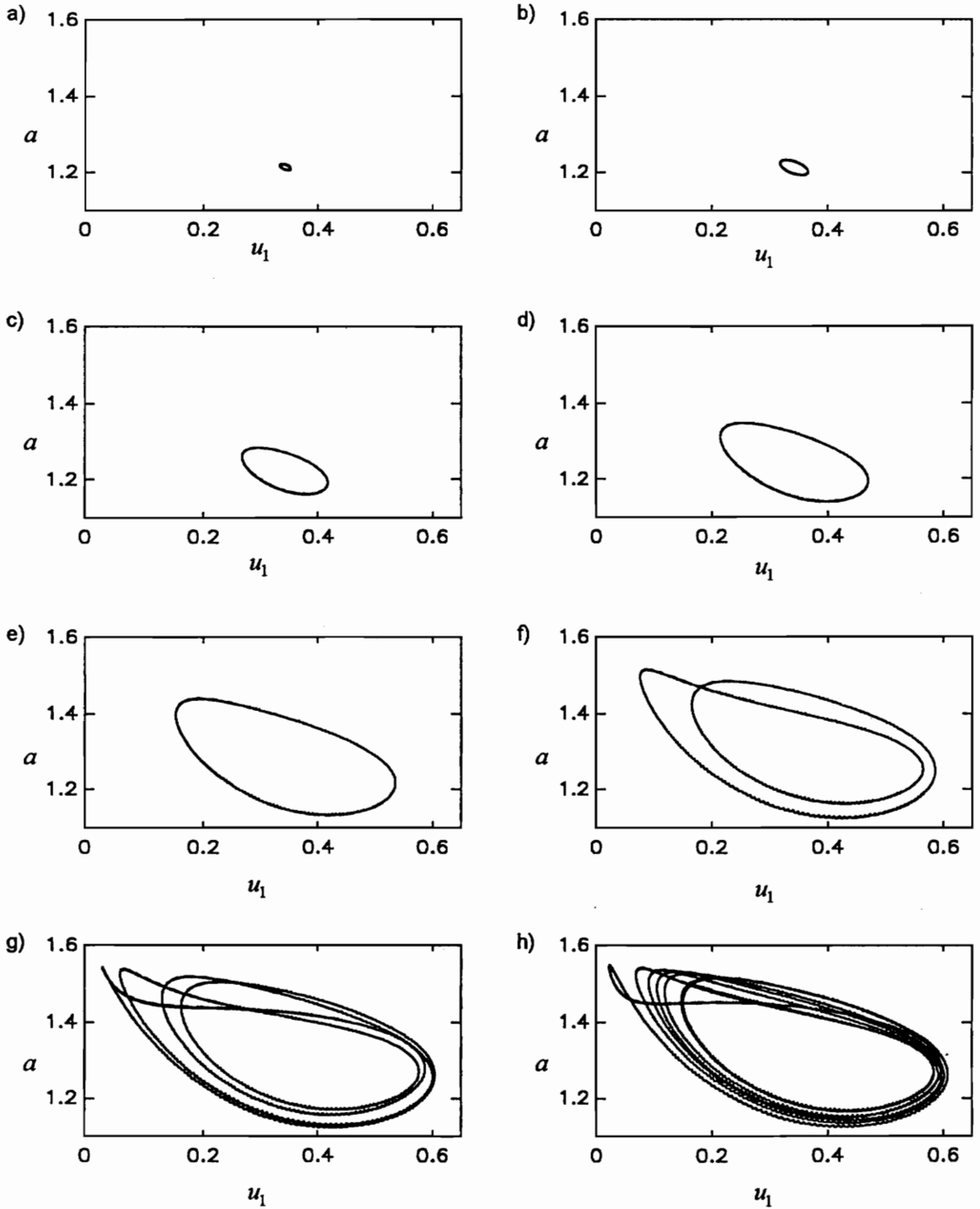
Fig. 4.10 Numerical simulation of the exact equations for $\varepsilon = 0.01$, $\alpha_1 = \alpha_3 = 1$, $\alpha_2 = -2$, $\alpha_4 = 3$, $\mu_1 = 0.25$, $\mu_2 = 0.5$, $f = 2.5$, and $\sigma =$ (a) 0.350, (b) 0.348, (c) 0.300, (d) 0.200, (e) 0.000, (f) –0.170, (g) –0.243, and (h) –0.260
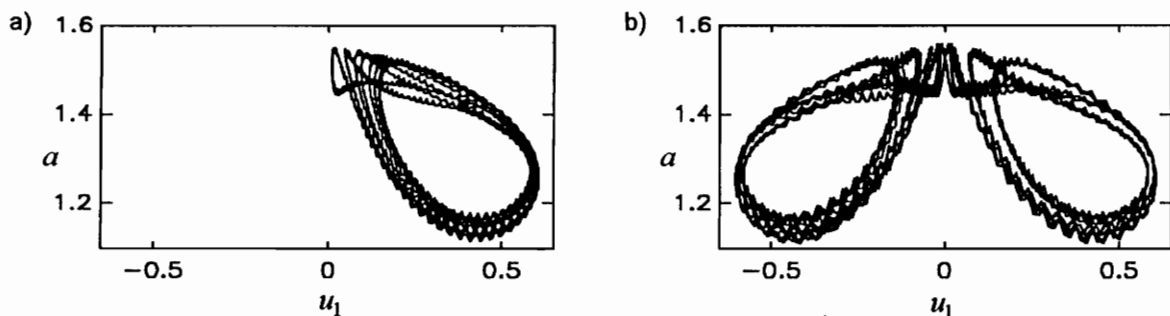
Fig. 4.11 Numerical simulation of the exact equations for $\alpha_1 = \alpha_3 = 1$, $\alpha_2 = -2$, $\alpha_4 = 3$, $\mu_1 = 0.25$, $\mu_2 = 0.5$, $f = 2.5$, $\sigma = -0.243$, and $\varepsilon =$ (a) 0.03 and (b) 0.05

in Fig. 4.7(g) is in good agreement with that shown in Fig. 4.10(g) where ϵ is 0.01. However, when ϵ is 0.03, as shown in Fig. 4.11(a) the exact equations yield a chaotic attractor in the right half-plane. For larger values of ϵ, a greater divergence between the results obtained from the averaged and exact equations occurs. When ϵ is 0.05, the exact equations yield a merged chaotic attractor rather than the period-four attractor which the averaged equations predict.

Nonetheless, the averaging approximation appears to be valid in most regimes for values of ϵ as large 0.05. The averaging procedure removes the high-frequency oscillations that are clearly visible on the trajectories for ϵ greater than or equal to 0.03. Naturally, as ϵ becomes larger and these oscillations increase in amplitude and decrease in frequency, the accuracy of the averaging approximation is expected to suffer.

4.6 Closure

In this chapter, the method of averaging was used to study a simple two-degree-of-freedom system with cubic nonlinearities. Like the system with quadratic nonlinearities studied in Chapter 2, this system exhibits an energy transfer from high- to low-frequency modes. However, the dynamics of this system are far more complicated

than those of the system considered in Chapter 2. Importantly, the results presented here indicate that the use of conventional methods to decrease a modal amplitude, such as increasing the damping coefficient or decreasing the excitation amplitude, may have undesirable effects.

CHAPTER 5

Modulated High-Frequency Excitation

5.1 Introduction

In this chapter, we consider a single-degree-of-freedom oscillator with cubic nonlinearity given by

$$\ddot{u} + 2\zeta\omega\dot{u} + \omega^2 u + \alpha\omega^2 u^3 = F(\omega t)\cos t \qquad (5.1)$$

where t is nondimensionalized so that the excitation frequency is unity and the natural frequency ω of the system is small. To show explicitly that the amplitude of the excitation F is slowly varying, we write it as a function of ωt.

We use the method of multiple scales to analyze the dynamics of the system and obtain a second-order nonlinear equation governing the low-frequency response of the system. This equation can be used to study the dynamics of the system for any slowly varying amplitude F. As a first example, we study the case where the amplitude is not modulated. We then treat the case of a harmonically modulated excitation for both weak and strong nonlinearity. This case is shown to be equivalent to the well known external combination resonance.

58

5.2 Perturbation Analysis

We determine a first-order approximation for the system response by the method of multiple scales (Nayfeh, 1981). We begin by introducing the new independent variables $T_0 = t$, $T_1 = \omega t$, and $T_2 = \omega^2 t$ which characterize, respectively, motion near the excitation frequency, near the natural frequency of the system, and at lower frequencies. Using the chain rule, we write the time derivative in terms of the T_i as

$$\frac{d}{dt} = D_0 + \omega D_1 + \omega^2 D_2 + \dots \tag{5.2}$$

where $D_n = \partial/\partial T_n$. We assume an expansion for u in the form

$$u(t) = u_0(T_0, T_1, T_2, \dots) + \omega u_1(T_0, T_1, T_2, \dots) + \omega^2 u_2(T_0, T_1, T_2, \dots) + \dots \tag{5.3}$$

Substituting Eqs. (5.2) and (5.3) into Eq. (5.1) and equating coefficients of equal powers of ω, we obtain

$$D_0^2 u_0 = F(T_1) \cos T_0 \tag{5.4}$$

$$D_0^2 u_1 = -2(D_0 D_1 u_0 + \zeta D_0 u_0) \tag{5.5}$$

$$D_0^2 u_2 = -\left[(D_1^2 + 2D_0 D_2) u_0 - 2D_0 D_1 u_1 + 2\zeta(D_1 u_0 + D_0 u_1) + u_0 + \alpha u_0^3 \right] \tag{5.6}$$

The general solution to Eq. (5.4) may be written as

$$u_0 = A(T_1, T_2) + B(T_1, T_2)T_0 - F(T_1) \cos T_0 \tag{5.7}$$

We require that the response be free of secular terms and therefore set $B = 0$. We note that, in Eq. (5.7), the term $F(T_1) \cos T_0$ represents the direct response to the high-frequency external forcing function and the term $A(T_1)$, which will be determined at higher order, captures low-frequency motion near the natural frequency of the system. We will find that, through the nonlinearity, the high-frequency motion can influence the low-frequency motion, causing resonant responses to occur under certain conditions.

Next, we substitute the expression for u_0 given in Eq. (5.7) into Eq. (5.5) and obtain

$$D_0^2 u_1 = -2(F' + \zeta F) \sin T_0 \tag{5.8}$$

whose solution is

$$u_1 = 2(F' + \zeta F) \sin T_0 \tag{5.9}$$

where the primes denote differentiation with respect to T_1. We have included only the particular solution because the homogeneous solution has the same form as A. At this order, no secular terms appear, and no information about A can be obtained.

Substituting Eqs. (5.7) and (5.9) into Eq. (5.6), we obtain

$$
\begin{aligned}
D_0^2 u_2 = & -A'' - 2F'' \cos T_0 - 2\zeta \left[A' + F' \cos T_0 + 2(\zeta F + F') \cos T_0 \right] \\
& -(A - F \cos T_0) - \alpha(A - F \cos T_0)^3
\end{aligned}
\tag{5.10}
$$

Secular terms are those which cause u_2 to grow without bound as $T_0 \to \infty$. In this case, the secular terms are the slowly varying terms. Eliminating them, we obtain the averaged equation governing A:

$$A'' + 2\zeta A' + \left(1 + \frac{3}{2}\alpha F^2\right) A + \alpha A^3 = 0 \tag{5.11}$$

For the purposes of this study, we will keep only the first two terms in the expansion and write

$$u = A - F \cos t + 2\omega(F' + \zeta F) \sin t + \ldots \tag{5.12}$$

Thus, the response of the system consists of components at the frequency of the excitation and a low-frequency component governed by Eq. (5.11). We note that the amplitude of the high-frequency excitation appears as a parametric excitation on the low-frequency component of the response and that therefore a modulated high-frequency excitation can cause resonant responses. Parametrically excited systems have been the subject of extensive study in recent years (e.g., Nayfeh and Mook, 1979; Ibrahim, 1986; and Schmidt and Tondl, 1986).

5.3 Response to Constant-Amplitude Excitation

Equation (5.11) can be used to study the dynamics of the system for any slowly varying amplitude F. In this section we consider the case where the excitation is not modulated (F is constant). In this case, Eq. (5.11) has the form of an unforced, damped, Duffing oscillator. If α is positive, A will always decay to zero. For negative α, unbounded motions are possible under two scenarios. If F^2 is greater in magnitude than $2/3\alpha$, the system is linearly unstable and the motion will be unbounded. If the foregoing condition is not satisfied, unbounded motions can still occur for sufficiently large initial conditions.

Phase portraits of A for $\alpha = -1$, light damping, and increasing values of F are shown in Fig. 5.1. In Fig. 5.1(a), $F = 0$ and the phase portrait is the same as would be obtained from Eq. (5.1). The portrait is dominated by the sink at $A = 0$ and the saddles at $A = \pm 1$. Any initial conditions between the insets of the saddles will lead to the sink at the origin. Outside this region, all initial conditions lead to unbounded motions. As the excitation amplitude is increased, the saddles move inward and the basin of attraction to the sink is considerably decreased as shown in Fig. 5.1(b). As F is increased beyond $\sqrt{2/3}$, the saddles converge to the sink and a reverse pitchfork bifurcation occurs. For larger values of F, the origin is linearly unstable and all initial conditions lead to unbounded motions, as shown in Fig. 5.1(c).

For oscillatory motions, the free-oscillation component of the response is not at the natural frequency of the system but rather its frequency is affected by the excitation as well as the nonlinearity. For weak nonlinearity (small α) or small amplitudes (small A), a perturbation method can be used to expand the averaged equation and determine the frequency of free oscillations.

For strong nonlinearity, we resort to numerical integration of Eq. (5.11) to compute the free-oscillation component of the response and then add particular solutions according to Eq. (5.12). In Fig. 5.2, we plot the undamped free response of the system for positive α and increasing values of F. We see that as F increases, the
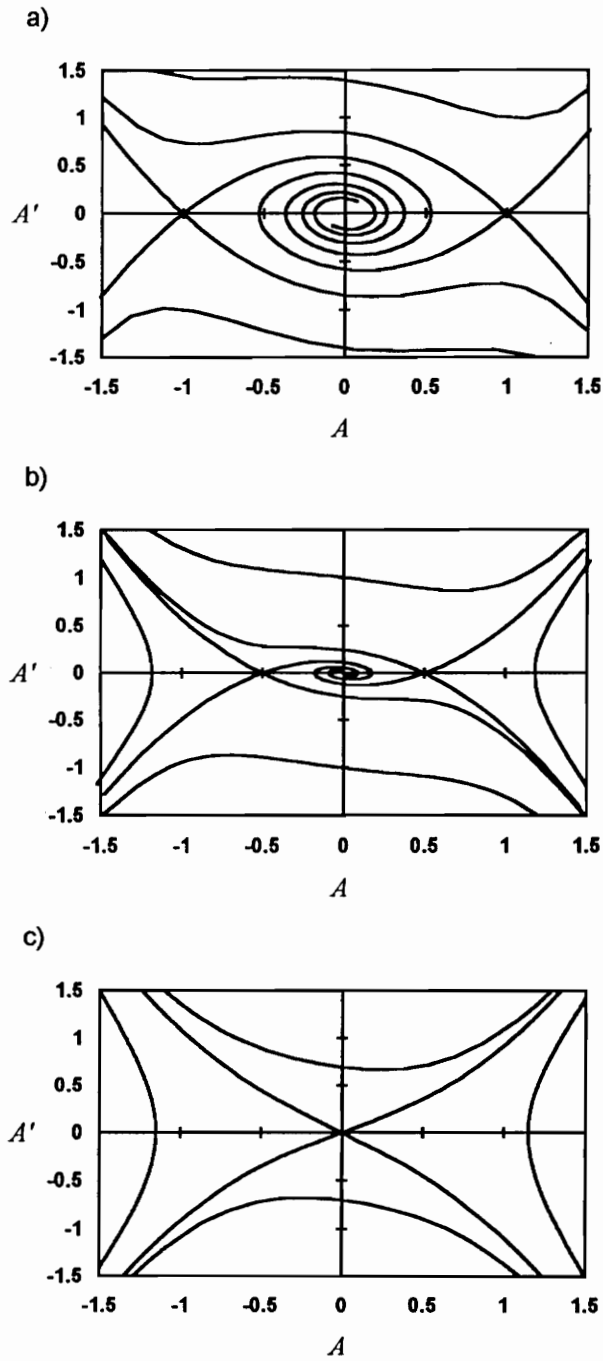
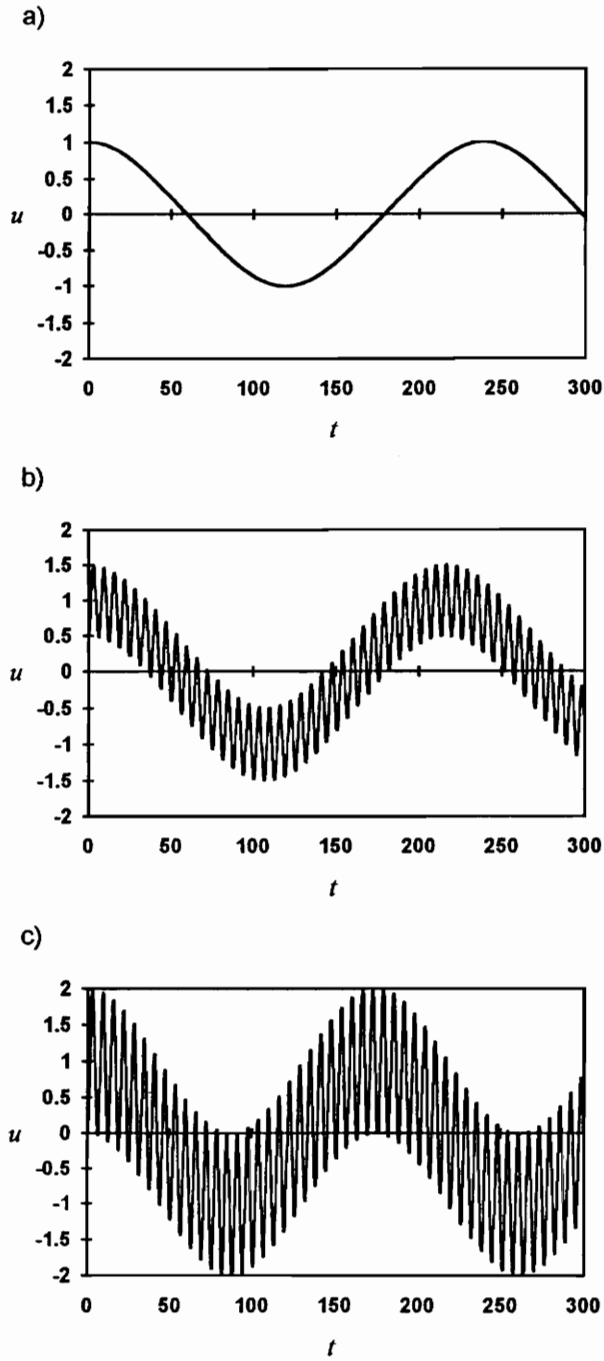Fig. 5.1   Phase portraits for $\alpha = -1.00$, $\mu = 0.10$, and $F =$ (a) 0.00, (b) 0.71, and (c) 1.00

Fig. 5.2   Free, undamped oscillations for $\omega = 0.02$, $\alpha = 1.00$, and $F =$ (a) 0.00, (b) 0.50, and (c) 1.00

frequency of the free-oscillation component of the response increases dramatically. Thus, the frequency of free oscillations can be controlled by modification of the excitation amplitude. This result is similar to that reported by Nayfeh and Mook (1979) for nonresonant hard excitations.

The perturbation approximation is valid for small ω. To investigate the validity of the averaged equation, we compare the free responses predicted by numerical integration of the full and averaged equations. In Fig. 5.3, we plot the predicted responses for $T_1 = 0$ to 6. For $\omega = 0.02$ (Fig. 5.3(a)), there is no visible difference between the two predictions. For larger ω, as shown in Figs. 5.3(b) and (c) for $\omega = 0.4$ and 0.6, respectively, the trajectories diverge at successively earlier times. This divergence confirms that increasing ω degrades the accuracy of the perturbation analysis.

5.4   Response to Harmonically Modulated Excitation

In this section, we study the case where the excitation amplitude undergoes simple-harmonic modulation. We therefore let

$$F = f + g \cos \Omega T_1 \tag{5.13}$$

We note that the excitation $F \cos t$ can in this case be written as a sum of harmonics as

$$f \cos t + \frac{1}{2} g \left[\cos(1 + \Omega \omega t) + \cos(1 - \Omega \omega t) \right] \tag{5.14}$$

Thus, the modulated excitation studied in this case can be viewed as a three-frequency excitation and the results interpreted as such.

5.4.1   Weak Nonlinearity

If the nonlinearity is weak and the damping is light, we can introduce ϵ to denote smallness and cast Eq. (5.11) in the weakly nonlinear form

$$A'' + 2\epsilon \zeta A' + \left[1 + \frac{3}{2} \epsilon \alpha F^2 \right] A + \epsilon \alpha A^3 = 0 \tag{5.15}$$
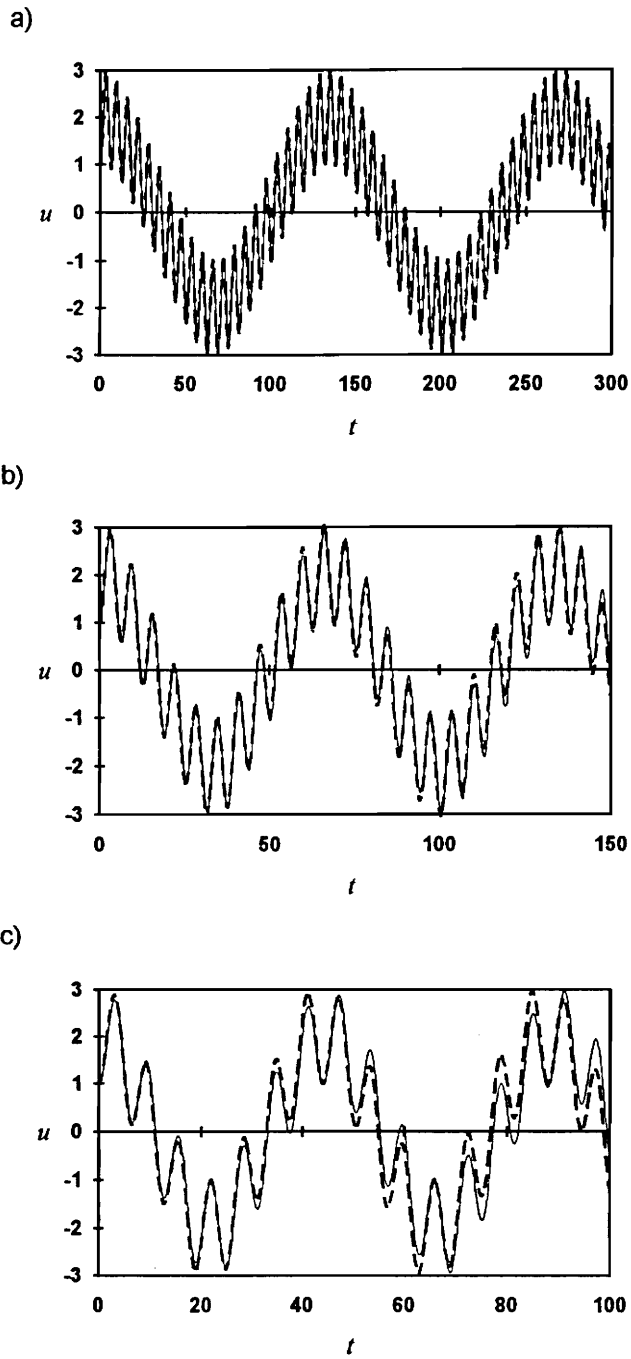
Fig. 5.3 Comparison of free, undamped oscillations predicted by the full (solid lines) and averaged (dashed lines) equations for $\alpha = 0.$, $F = 1.0$, and $\omega =$ (a) 0.02, (b) 0.04, and (c) 0.06

where we will later set $\epsilon = 1$.

We now apply the method of multiple scales to Eq. (5.15) by introducing the independent variables $\tau_0 = T_1$ and $\tau_1 = \epsilon T_1$ and expanding A in the form

$$A(T_1) = A_0(\tau_0, \tau_1, \ldots) + \epsilon A_1(\tau_0, \tau_1, \ldots) + \ldots \qquad (5.16)$$

Equating equal powers of ϵ, we obtain

$$\Delta_0^2 A_0 + A_0 = 0 \qquad (5.17)$$

$$\Delta_0^2 A_1 + A_1 = -2\Delta_0\Delta_1 A_0 - 2\zeta\Delta_0 A_0 - \frac{3}{2}\alpha F^2 A_0 - \alpha A_0^3 \qquad (5.18)$$

where $\Delta_n = \partial/\partial\tau_n$. The general solution of Eq. (5.17) can be written as

$$A = G(\tau_1)e^{i\tau_0} + \bar{G}(\tau_1)e^{-i\tau_0} \qquad (5.19)$$

where the bar denotes complex conjugation. Substituting Eq. (5.19) into Eq. (5.18), we obtain

$$\Delta_0 A_1 + A_1 = -2(iG' + i\zeta G + \frac{3}{2}\alpha G^2\bar{G})e^{i\tau_0} - \alpha G^3 e^{3i\tau_0} + cc \qquad (5.20)$$
$$-\frac{3}{2}\alpha F^2 \left(Ge^{i\tau_0} + \bar{G}e^{-i\tau_0} \right)$$

where cc denotes the complex conjugate of preceding terms. In order to eliminate secular terms and determine an equation governing G, we must choose a form for F.

Substituting the specific form for F given in Eq. (5.13) into Eq. (5.20), we find that, to this order, resonances may occur if Ω is near either 1 or 2. These conditions correspond to modulation frequencies near ω and 2ω. A higher-order analysis would predict the occurrence of resonances for other values of Ω. In this section, we consider the case where $\Omega \approx 1$ and therefore set $\Omega = 1 + \epsilon\sigma$. Eliminating secular terms from Eq. (5.20), we obtain the following modulation equation governing G:

$$2iG' + 2\left[i\zeta + \frac{3}{8}\alpha\left(2f^2 + g^2\right)\right]G + \frac{3}{8}\alpha g^2\bar{G}e^{2i\sigma\tau_1} + 3\alpha G^2\bar{G} = 0 \qquad (5.21)$$

Here, we note that Eq. (5.21) has the same form as those obtained by previous researchers in the study of combination resonances (e.g., Nayfeh, 1985).

Next, we separate the modulation equation into real and imaginary parts by writing G in terms of an amplitude and phase as

$$G = \frac{1}{2} a e^{i(\sigma\tau_1 - \beta)} \tag{5.22}$$

Substituting this expression into Eq. (5.21), we obtain the autonomous system of equations

$$a' = -\zeta a - \frac{3}{16}\alpha a g^2 \sin 2\beta \tag{5.23}$$

$$a\beta' = \sigma a - \frac{3}{8}\alpha(2f^2 + g^2)a - \frac{3}{16}\alpha a g^2 \cos 2\beta - \frac{3}{8}\alpha a^3 \tag{5.24}$$

Setting $\epsilon = 1$, we now write the system response as

$$u = a\cos(\omega\Omega t + \beta) - F\cos t + 2\omega(F' + \zeta F)\sin t + \ldots \tag{5.25}$$

Steady-state solutions of A satisfy $a' = \beta' = 0$. Solving for a, we find that $a = 0$ or

$$a = \left\{ \frac{8\sigma}{3\alpha} - (2f^2 + g^2) \pm \frac{8}{3\alpha}\left[\left(\frac{3}{16}\alpha g^2\right)^2 - \zeta^2 \right]^{\frac{1}{2}} \right\}^{\frac{1}{2}} \tag{5.26}$$

Stability of these fixed-point solutions can be determined from the eigenvalues of the Jacobian matrix of Eqs. (5.23) and (5.24) evaluated at the fixed points.

In Fig. 5.4, we plot frequency-response curves of a for positive α and various values of the constant component of the excitation f. The frequency-response curves have the same shape as would be obtained for a nonlinear Mathieu equation, but they are shifted strongly to the right as f is increased. The results presented in Fig. 5.4 indicate that, under some conditions, an increase in f can cause a decrease in the low-frequency response amplitude a.

We plot a as a function of f in Fig. 5.5. We see that at $f = 0$ both a trivial and a nontrivial solution are possible. As f is increased, the nontrivial solution decreases in amplitude and the trivial solution loses stability, causing a jump to the nontrivial branch. As f is further increased, the nontrivial solution approaches zero sharply. For large enough values of f, only trivial solutions are possible. This figure shows
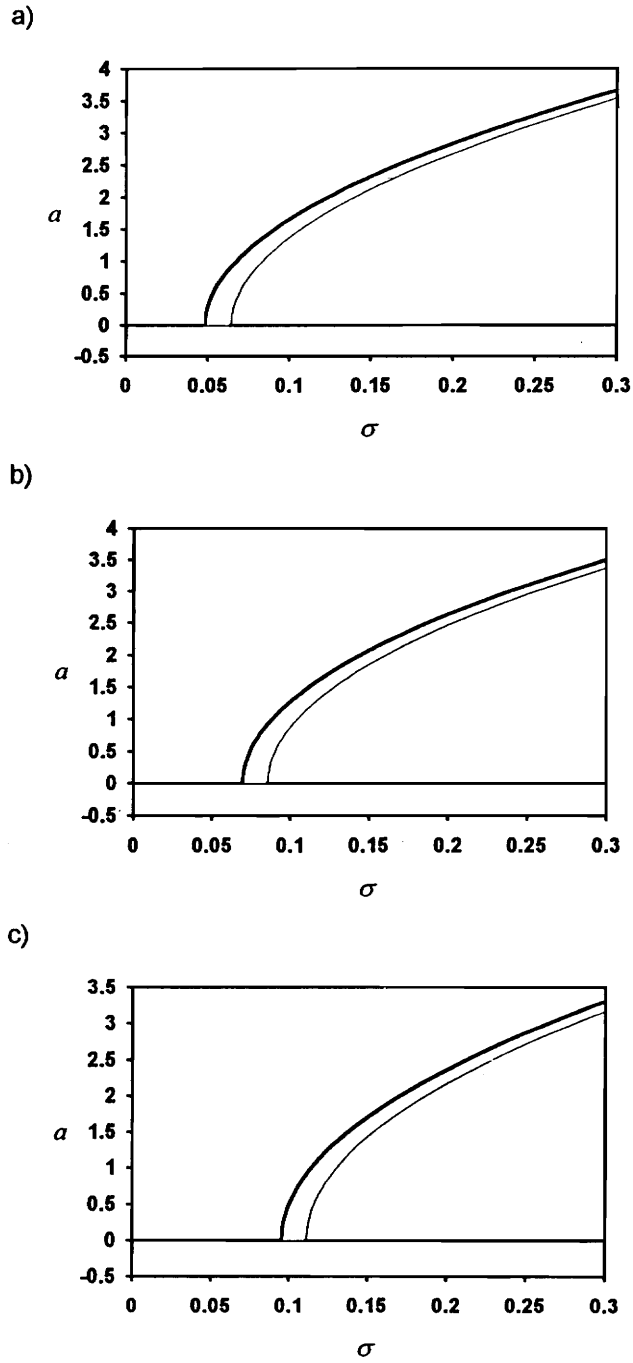
Fig. 5.4 Frequency-response curves for $\alpha = 0.05$, $\zeta = 0.005$, $g = 1.00$, and $f =$ (a) 1.00, (b) 1.25, and (c) 1.50
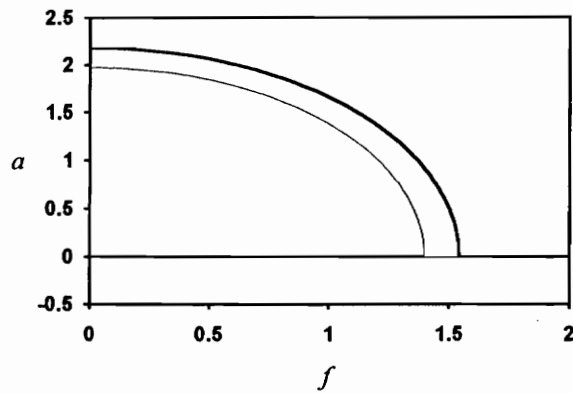
Fig. 5.5 Amplitude of low-frequency response as a function of f for $\alpha = 0.05$, $\zeta = 0.005$, $\sigma = 0.10$, and $g = 1.00$

clearly that an increase in the amplitude of the constant component of the excitation can decrease the amplitude of the low-frequency response. However, because the high-frequency component of the response is proportional to f, the total response amplitude does not decrease as f is increased.

Whereas the only effect of f on the amplitude a of the low-frequency response is to cause a frequency shift, the term $g \cos \Omega T_1$ pumps energy into the low-frequency oscillations and causes a frequency shift. Neither effect is dominant and we find therefore that the dependence of a on g is not simple. In Fig. 5.6, we plot a as a function of g while holding σ constant. As expected, only the trivial solution is possible for small g. As we increase g from this level, a jump to the nontrivial solution occurs. We find however that as g is further increased, the nontrivial solution goes to zero and beyond that point only the trivial solution is possible.

The case of $\Omega \approx 1$ studied in this section corresponds to the case where the frequency of modulation is near the frequency of free oscillation as shown in the time trace of Fig. 5.7. Other resonances are possible and can be predicted using a higher order analysis than was presented in this section. In the next section, we present numerical examples of some of these resonances for large values of α.
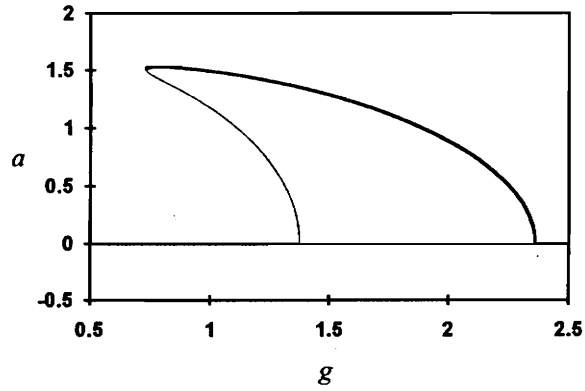
Fig. 5.6   Amplitude of low-frequency response as a function of g for $\alpha = 0.05$, $\zeta = 0.005$, $\sigma = 0.09$, and $f = 1.00$
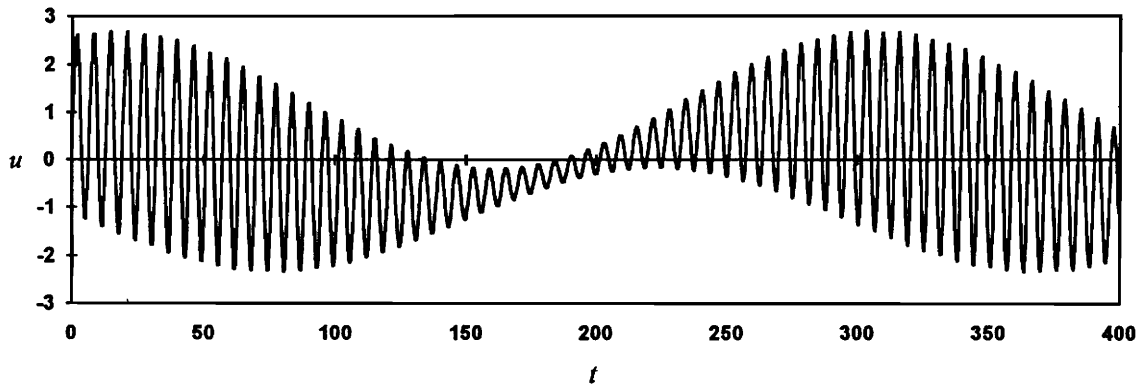

Fig. 5.7   Time trace of the response for $\alpha = 0.05$, $\zeta = 0.005$, $\sigma = 0.08$, $\omega = 0.02$, $f = 1.25$, and $g = 1.00$

Modulated High-Frequency Excitation   70
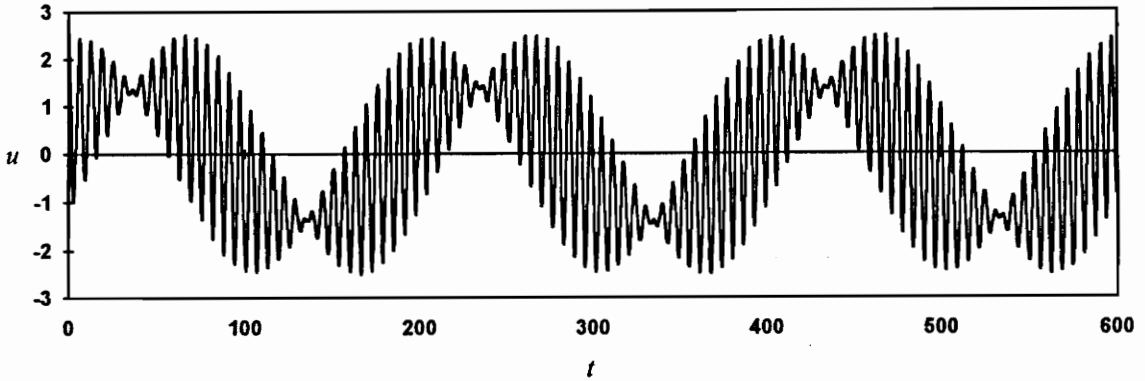
Fig. 5.8   Time trace of the response for $\alpha = 0.50$, $\zeta = 0.01$, $\Omega = 1.58$, $f = 0.00$, and $g = 2.00$

5.4.2   Strong Nonlinearity

Here, we consider the case where the nonlinearity is strong. In this case, perturbation methods are ineffective for the study of the averaged equation, Eq. (5.11), and we resort to numerical integration. This approach has considerable advantages over integration of the full equation, Eq. (5.1). Because the averaged equation contains only low frequencies, a much larger time-step can be used than in the case of the full equation. Moreover, the responses obtained from the averaged equation are far more easily identified than those obtained from the full equation because they do not contain the high-frequency components which can muddy phase portraits and Poincaire sections.

If $f = 0$, Eq. (5.11) can be rewritten as a nonlinear Mathieu equation

$$A'' + 2\zeta A' + \left(1 + \frac{3}{4}\alpha g^2 + \frac{3}{4}\alpha g^2 \cos 2\Omega T_1\right) A + \alpha A^3 = 0 \qquad (5.27)$$

which has been studied extensively in the literature. Linearizing, we find that the frequency of undamped infinitesimal free oscillations is $(1 + 3\alpha g^2/4)^{1/2}$.

The strongest resonance will occur if Ω is near this frequency. This case was treated in the previous section for weak nonlinearity. The motion in this case is shown in Fig. 5.8, and it can be seen that the low-frequency response undergoes one
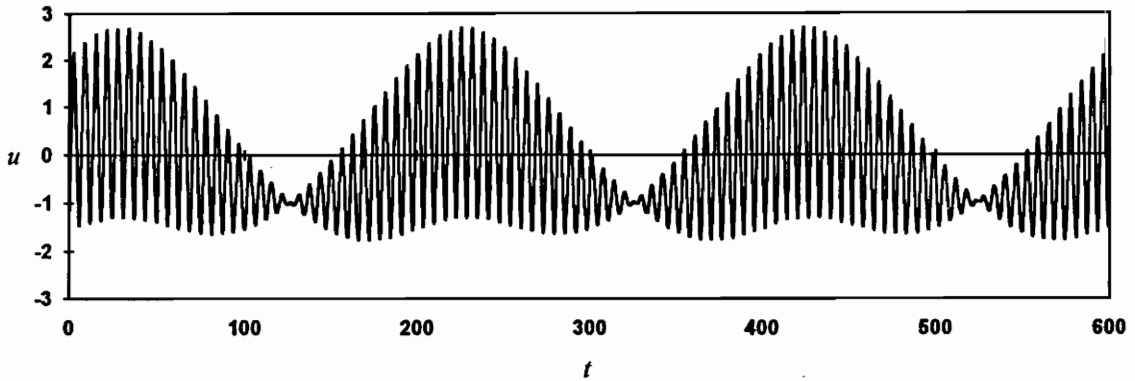
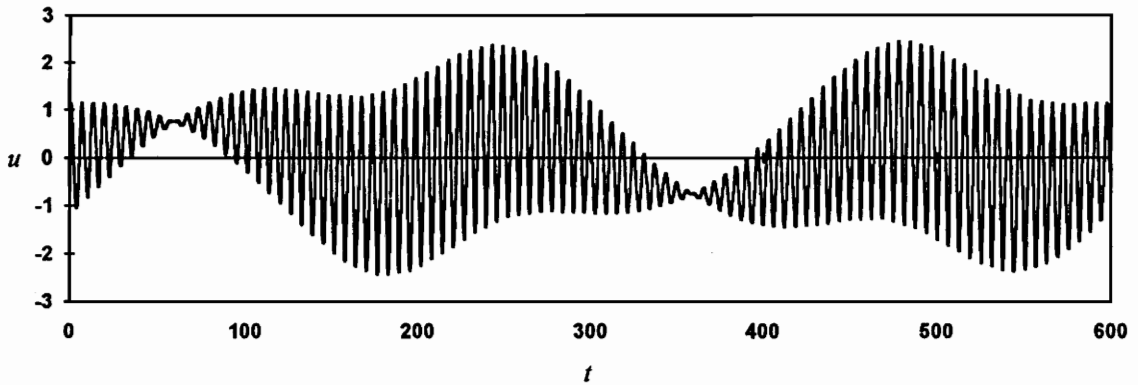Fig. 5.9 Time trace of the response for $\alpha = 0.50$, $\zeta = 0.01$, $\Omega = 0.79$, $f = 0.00$, and $g = 2.00$

Fig. 5.10 Time trace of the response for $\alpha = 0.50$, $\zeta = 0.01$, $\Omega = 0.53$, $f = 0.00$, and $g = 2.00$

cycle for every cycle of the high-frequency response (two beats). Other resonances may occur if Ω is near one-half or one-third of the frequency of free oscillations. These cases are shown in Figs. 5.9 and 5.10, respectively.

5.5   Closure

In this chapter, the response of a single-degree-of freedom system with cubic nonlinearities to a modulated high-frequency input was studied. The method of multiple scales was used to derive a second-order equation governing the components of the

response of the system near its natural frequency. In this equation, the amplitude of the excitation, which is a function of time, appears as a parametric excitation.

The result of the perturbation analysis was used to study the response of the system to constant-amplitude and harmonically modulated excitations. For harmonically modulated excitations, various resonances occur and these were shown to correspond to external combination resonances. These examples are fairly straightforward, but more difficult problems involving aperiodic modulation could be studied with the analysis presented here.

CHAPTER 6

Discussion and Conclusions

6.1 Discussion of the Current Work

In this thesis, we investigated the nonlinear dynamics of systems where some compo-
nents of the response evolve on the slow time scale and others evolve on the fast time
scale. It was found that such systems exhibit a range of phenomena not observed in
systems where all components evolve on the same time scale, the most significant of
which is the energy transfer from high- to low-frequency modes.

This energy transfer is a consequence of the strong coupling between modes evolv-
ing on different time scales which is similar to the strong coupling that exists between
modes with a 1:3 frequency ratio in systems with cubic nonlinearities. The resulting
internal resonance is often referred to as a 1:3 autoparametric resonance. Because the
natural frequency of a mode that evolves on the slow time scale is nearly zero, the
interaction between slow and fast time scales may be viewed as a 0:1 autoparametric
resonance.

In contrast to the interactions due to the well-known parametric, external, and
classical internal resonances, the interactions between the low- and high-frequency
modes do not require the existence of any precise frequency relationships in the sys-
tem. Rather, it seems that these interactions can occur if there exist modes whose

74

natural frequencies are much lower than the natural frequencies of the modes being directly driven. Also, in contrast to interactions caused by the occurrence of broadband chaos, the interactions described here can occur whenever the amplitudes and phases of the high-frequency modes undergo slow modulations.

One aspect of the response of systems with widely spaced modes that has not been emphasized thus far is the occurrence of static deflections in the low-frequency modes, which were found to occur even in the absence of even nonlinearities. These static deflections may be particularly significant in applications such as robotics where the position of a mechanism must be controlled with precision.

The transfer of energy from high- to low-frequency vibrations studied in this thesis is of great practical importance. In many engineering systems, high-frequency excitations can be caused by rotating machinery. Through the mechanisms investigated in this thesis, energy from these high-frequency sources can be transferred to low-frequency modes of supporting structures or foundations, resulting in dangerously large oscillations. Moreover, the results presented in Chapters 4 and 5 indicate that the use of conventional methods for the decrease of a mode's response, such as increasing the dissipation or decreasing the force amplitude, may actually increase the amplitude of the low-frequency response.

6.2 Suggestions for Future Work

There are many aspects of the dynamics of systems with widely spaced frequencies that are not yet understood. Free oscillations of systems with widely spaced modes have not yet been investigated although they promise to show some very unusual features. The concept of a nonlinear mode shape has gained much interest recently; nonlinear mode shapes of systems with widely spaced modes may exhibit mode bifurcations and static streaming in the absence of even nonlinearities.

Thus far, only systems involving one low-frequency mode have been analyzed, but two low-frequency modes were excited in the experiment of Chapter 2. It would be

useful to study which of the lowest modes of any given structure may be excited when a high-frequency mode is driven. Other systems that may be studied include systems where excitations are applied on both the slow and fast time scales. In such cases, an energy exchange between the modes should occur but it may be more difficult to characterize.

REFERENCES

Anderson, T. J., Balachandran, B., and Nayfeh, A. H., 1992, "Observations of Nonlinear Interactions in a Flexible Cantilever Beam," AIAA Paper No. 92–2332, *Proceedings of the 33rd AIAA Structures, Structural Dynamics, and Materials Conference*, Dallas, TX.

Anderson, T. J., Nayfeh, A. H., and Balachandran, B., 1993, "Coupling Between Widely Spaced Modes and a Low-Frequency Mode: Theory and Experiment," *Nonlinear Dynamics*, submitted.

Bajaj, A. K., and Johnson, J. M., 1990, "Asymptotic Techniques and Complex Dynamics in Weakly Non-Linear Forced Mechanical Systems," *International Journal of Non-Linear Mechanics*, Vol. 25, pp. 211–226.

Burton, T. D., and Kolowith, M., 1988, "Nonlinear Resonances and Chaotic Motion in a Flexible Parametrically Excited Beam," *Proceedings of the Second Conference on Non-linear Vibrations, Stability, and Dynamics of Structures and Mechanisms*, Blacksburg, VA.

Colbert, M. A., 1990, "An Optical System for Three-Dimensional Motion Measurement," M. S. Thesis, Department of Electrical Engineering, Virginia Polytechnic Institute and State University, Blacksburg, VA.

Crespo da Silva, M. R. M., 1980, "On the Whirling of a Base Excited Cantilever Beam," *Journal of the Acoustical Society of America*, Vol. 67, pp. 707–740.

Cusumano, J. P., and Moon, F. C., 1989, "Low Dimensional Behavior in Chaotic Nonplanar Motions of a Forced Elastic Rod: Experiment and Theory," *Nonlinear Dynamics in Engineering Systems, IUTAM Symposium*, Germany.

Dugundji, J., and Mukhopadhyay, V., 1973, "Lateral Bending-Torsion Vibrations of a Thin Beam Under Parametric Excitation," *Journal of Applied Mechanics*, Vol. 40, pp. 693–698.

Guckemheimer, J., and Holmes, P., 1983, *Nonlinear Oscillations, Dynamical Systems, and Bifurcation of Vector Fields*, Springer-Verlag, New York.

Haddow, A. G., and Hasan, S. M., 1988, "Nonlinear Oscillations of a Flexible Cantilever: Experimental Results," *Proceedings of the Second Conference on Nonlinear Vibrations, Stability, and Dynamics of Structures and Mechanisms*, Blacksburg, VA.

Haight, E. C., and King, W. W., 1972, "Stability of Non-Linear Oscillations of an Elastic Rod," *Journal of the Acoustical Society of America*, Vol. 52, pp. 899–911.

Hyer, M. W., 1979, "Whirling of a Base-Excited Cantilever Beam," *Journal of the Acoustical Society of America*, Vol. 65, pp. 931–939.

Ibrahim, R. A., 1985, *Random Parametric Vibration*, Wiley, New York.

Nayfeh, A. H., 1973, *Perturbation Methods*, Wiley-Interscience, New York.

Nayfeh, A. H., 1981, *Introduction to Perturbation Techniques*, Wiley- Interscience, New York.

Nayfeh, A. H., 1985, "The Response of Non-Linear Single-Degree-of-Freedom Systems to Multifrequency Excitations," *Journal of Sound and Vibration*, Vol. 102, pp. 403-414.

Nayfeh, A. H., and Balachandran, B., 1989, "Modal Interactions in Dynamical and Structural Systems," *Applied Mechanics Reviews*, Vol. 42, pp. S175-S201.

Nayfeh, A. H., and Jebril, A. E. S., 1987, "The Response of Two-Degree-of- Freedom Systems with Quadratic and Cubic Nonlinearities to Multifrequency Excitations," *Journal of Sound and Vibration*, Vol. 115, pp. 83-101.

Nayfeh, A. H., and Mook, D. T., 1979, *Nonlinear Oscillations*, Wiley- Interscience, New York.

Pai, P. F., and Nayfeh, A. H., 1990, "Nonlinear Non-Planar Oscillations of a Cantilever Beam Under Lateral Base Excitations," *International Journal of Non-Linear Mechanics*, Vol. 25, pp. 455–474.

Schmidt, G., and Tondl, A., 1986, *Non-Linear Vibrations*, Akademie-Verlag, Berlin.

Shyu, I.-M. K., Mook, D. T., and Plaut, R. H., 1993, "Whirling of a Forced Cantilevered Beam with Static Deflection. I: Primary Resonance," *Nonlinear Dynamics*, in press.

VITA

The author was born in Mountain View, California on July 1, 1970. In 1971, he relocated with his family to Blacksburg, Virginia and has remained there through the completion of this document and the attainment of his M. S. degree in Engineering Mechanics at VPI & SU in 1993. He began his education at the VPI & SU preschool, received his primary education at Harding Avenue Elementary School, served a four-year sabbatical at Yarmouk University Model School, attended Blacksburg High School for three years, and then went on to earn a B. S. degree in Engineering Science and Mechanics at VPI & SU in 1991.